Cell

Antitelomerase Therapy Provokes ALT and Mitochondrial Adaptive Mechanisms in Cancer

Jian Hu,[1,4,5,6] Soyoon Sarah Hwang,[1,4,5] Marc Liesa,[8] Boyi Gan,[3,4,5,6] Ergun Sahin,[4,5,6] Mariela Jaskelioff,[4,5,6] Zhihu Ding,[4,5,6] Haoqiang Ying,[1,4,5,6] Adam T. Boutin,[1,4,5,6] Hailei Zhang,[4,5] Shawn Johnson,[5] Elena Ivanova,[4,5] Maria Kost-Alimova,[1,4,5] Alexei Protopopov,[1,4,5] Yaoqi Alan Wang,[1,4,5] Orian S. Shirihai,[8] Lynda Chin,[2,4,5,7] and Ronald A. DePinho[1,4,5,6,*]

[1]Department of Cancer Biology
[2]Department of Genomic Medicine
[3]Department of Experimental Radiation Oncology
University of Texas MD Anderson Cancer Center, Houston, TX 77030, USA
[4]Belfer Institute for Applied Cancer Science
[5]Department of Medical Oncology
Dana-Farber Cancer Institute, Boston, MA 02115, USA
[6]Department of Genetics and Medicine
[7]Department of Dermatology
Harvard Medical School, Boston, MA 02115, USA
[8]Department of Medicine, Boston University School of Medicine, Boston, MA 02118, USA
*Correspondence: rdepinho@mdanderson.org
DOI 10.1016/j.cell.2011.12.028

SUMMARY

To assess telomerase as a cancer therapeutic target and determine adaptive mechanisms to telomerase inhibition, we modeled telomerase reactivation and subsequent extinction in T cell lymphomas arising in *Atm*$^{-/-}$ mice engineered with an inducible telomerase reverse transcriptase allele. Telomerase reactivation in the setting of telomere dysfunction enabled full malignant progression with alleviation of telomere dysfunction-induced checkpoints. These cancers possessed copy number alterations targeting key loci in human T cell lymphomagenesis. Upon telomerase extinction, tumor growth eventually slowed with reinstatement of telomere dysfunction-induced checkpoints, yet growth subsequently resumed as tumors acquired alternative lengthening of telomeres (ALT) and aberrant transcriptional networks centering on mitochondrial biology and oxidative defense. ALT+ tumors acquired amplification/overexpression of PGC-1β, a master regulator of mitochondrial biogenesis and function, and they showed marked sensitivity to PGC-1β or SOD2 knockdown. Genetic modeling of telomerase extinction reveals vulnerabilities that motivate coincidental inhibition of mitochondrial maintenance and oxidative defense mechanisms to enhance antitelomerase cancer therapy.

INTRODUCTION

Telomeres are nucleoprotein complexes at chromosome ends that function to maintain chromosomal integrity. Genetic models have defined their critical roles in cancer (Artandi and DePinho, 2010), aging, and degenerative diseases (Sahin and DePinho, 2010). Telomeres are synthesized by telomerase consisting of a reverse transcriptase catalytic subunit (TERT) and an RNA template subunit (TERC) (Feng et al., 1995; Nakamura et al., 1997). As normal or premalignant cells divide, the end-replication problem of conventional DNA polymerases, coupled with low or absent telomerase activity, results in loss of telomere sequences and eventual telomere uncapping, which activates cellular checkpoints similar to those provoked by DNA double-stranded-breaks (DSBs) (Harley and Sherwood, 1997). Like classical DSBs, telomere dysfunction has been shown to induce p53 and associated cellular responses, such as senescence and/or apoptosis (Chin et al., 1999; d'Adda di Fagagna et al., 2003; Karlseder et al., 1999; Takai et al., 2003; van Steensel et al., 1998). Upon mutational inactivation of p53, continued cell cycling and survival of cells with telomere dysfunction provide a procarcinogenic mutator mechanism characterized by translocations and regional amplifications and deletions (Artandi et al., 2000; Chin et al., 1999; O'Hagan et al., 2002). At the same time, persistent telomere dysfunction and associated rampant chromosomal instability (even in p53 null cells) compromises cellular viability (Begus-Nahrmann et al., 2009; Chin et al., 1999) and constrains full malignant progression of such cancers (Artandi et al., 2000; Chang et al., 2003; González-Suárez et al., 2000; Rudolph et al., 2001).

The occurrence of telomere erosion and importance of telomerase-mediated telomere maintenance in fully established cancers are evidenced by typically short telomeres relative to normal tissues and robust telomerase activity in most human cancers (Shay and Wright, 2006). This profile of shorter telomeres and telomerase activity in cancer has motivated the clinical development of telomerase inhibitors including a 13-mer antisense oligonucleotide in a number of cancer types (Agrawal et al., 2012; Shay and Wright, 2006). At present, uncertainty surrounds whether antitelomerase therapy will be hampered by the potential lag time needed for telomere erosion-associated tumor cell killing, and/or whether re-entry into telomere-based crisis will engender genomic instability that may allow for emergence of adaptive responses and resistance mechanisms, such as alternative lengthening of telomeres (ALT) mechanism which enables telomere maintenance via homologous recombination (Cesare and Reddel, 2010). Notably, in *mTERC*$^{-/-}$ mice, p53 deficiency alleviates tumor suppression imparted by telomere dysfunction (Chin et al., 1999) and, in transformed cells with intact p53-dependent DNA damage checkpoint, there is activation of ALT (Chang et al., 2003).

The study of cancer pathogenesis and specific role of telomeres therein have been enabled by the use of genetically engineered mouse models of cancer, which provide an in vivo assessment of the complex adaptive responses to targeted cancer treatments. Here, we exploited the experimental merits of mice to model and study more precisely telomere crisis, telomerase reactivation and telomerase extinction in cancer development, progression and treatment in the in vivo setting. To that end, we engineered an inducible *TERT* knockin allele and studied telomere dynamics in mice mutant for *Atm*, which develop T cell lymphomas with high penetrance (Xu et al., 1996). The *Atm* mutant model was selected to study telomerase activation and its extinction as this model retains a robust p53-mediated checkpoint response upon telomere uncapping which strongly suppresses emergent tumors (Qi et al., 2003; Wong et al., 2003). Our study provides in vivo genetic evidence that telomerase reactivation facilitates the progression of spontaneous arising tumors experiencing telomere dysfunction and, conversely, that telomerase extinction in established cancers activates ALT and other adaptive mechanisms, illuminating potential therapeutic combinations.

RESULTS

Telomerase Reactivation Promotes Tumorigenesis by Stabilizing Telomeres and Alleviating Telomere Dysfunction-Induced Checkpoints

We generated mice harboring an *Atm* null allele (Xu et al., 1996) and a 4-Hydroxytamoxifen (4-OHT)-inducible *Telomerase Reverse Transcriptase-Estrogen Receptor* (*TERT-ER*^{T2}) fusion knockin allele (Jaskelioff et al., 2011). In the absence of 4-OHT, mice homozygous for *TERT*^{ER} (designated *TERT*$^{ER/ER}$) are telomerase activity deficient and sustain same cytogenetic and cellular phenotypes of conventional *TERT* or *TERC* knockout model (Jaskelioff et al., 2011). Upon 4-OHT treatment, TERT-ER protein activity can be restored to levels comparable to the native TERT protein (Jaskelioff et al., 2011). To generate lymphoma-prone mice with telomere dysfunction, *Atm*$^{+/-}$ *TERT*$^{+/ER}$ mice were intercrossed to produce first generation (G_1) *Atm*$^{-/-}$*TERT*$^{ER/ER}$ and *Atm*$^{+/-}$*TERT*$^{ER/ER}$ mice. G_1 *Atm*$^{+/-}$*TERT*$^{ER/ER}$ mice were then serially intercrossed to successive generations in the absence of 4-OHT, culminating in G_3 and G_4 *Atm*$^{-/-}$*TERT*$^{ER/ER}$ experimental cohorts (Figure S1A available online). For brevity, the *Atm*$^{-/-}$ *TERT*$^{+/+\ or\ +/ER}$, G_1 *Atm*$^{-/-}$ *TERT*$^{ER/ER}$, and $G_{3\text{-}4}$ *Atm*$^{-/-}$*TERT*$^{ER/ER}$ mice are designated G_0, G_1, and $G_{3\text{-}4}$, respectively.

G_0 and G_1 mice developed T cell lymphomas at similar latencies and penetrance (Figure S1B), which is consistent with adequate telomere reserves to maintain capping in G_1 mice and avoid activated DNA damage checkpoints. In contrast, $G_{3\text{-}4}$ lymphomas emerge with a longer latency and lower penetrance relative to G_1 controls (Figure 1A), consistent with previous work (Maser et al., 2007; Qi et al., 2003; Wong et al., 2003). Next, to test the impact of telomerase reactivation on lymphoma kinetics in this model, continuous-release 4-OHT tablets were implanted subcutaneously at 18 weeks, an age when lymphomas in *Atm*$^{-/-}$ mice with intact telomeres start to emerge. 4-OHT-treated $G_{3\text{-}4}$ mice developed overt lymphomas more rapidly and with higher penetrance than, not only vehicle-treated $G_{3\text{-}4}$ mice, but also G_1 mice (Figure 1A). In contrast, there were no differences in tumor latency and penetrance in the 4-OHT- and vehicle-treated G_1 mice (Figure 1A). On the histopathological level, vehicle-treated $G_{3\text{-}4}$ tumors were smaller in size and displayed less aggressive malignant features relative to 4-OHT-treated $G_{3\text{-}4}$ tumors as well as telomere intact G_0 and G_1 tumors (Figures 1B–1D; data not shown). Finally, 4-OHT treatment itself does not impact on lymphomagenesis as reflected by similar survival curves of $G_{3\text{-}4}$ *Atm*$^{-/-}$ *TERT*$^{ER/ER}$ *mTR*$^{-/-}$ mice treated with either vehicle or 4-OHT (Figure 1A), supporting the view that acceleration of 4-OHT on $G_{3\text{-}4}$ *Atm*$^{-/-}$*TERT*$^{ER/ER}$ tumors stems from telomerase reactivation and not from nontelomere activities of 4-OHT.

The capacity to regulate endogenous telomerase activity in vivo prompted serial analyses of malignant properties and cellular checkpoint responses as functional readouts of telomere status during lymphomagenesis and progression in $G_{3\text{-}4}$ mice. Quantitation of DNA damage foci by anti-γH2AX and -53BP1 staining showed markedly increased foci in vehicle-treated $G_{3\text{-}4}$ tumor cells and a dramatic decrease in such foci in 4-OHT-treated $G_{3\text{-}4}$ tumor cells (Figures 2A and 2B; Figure S2). Correspondingly, vehicle-treated $G_{3\text{-}4}$ tumor cells exhibited decreased proliferation (Ki67) and increased apoptosis (cleaved caspase 3), senescence (SA-β-Gal), and p53 signaling (p53 phosphorylation and p21 expression), which are all alleviated by telomerase reactivation (Figures 2C–2F).

Telomerase Reactivation in Spontaneous Tumors with Unstable Genomes Promotes Aggressive Malignant Properties

A higher percentage of $G_{3\text{-}4}$-4-OHT mice exhibited widespread tumor cell infiltration in spleen, kidney, liver, lung, and bone marrow relative to vehicle-treated $G_{3\text{-}4}$ mice as well as 4-OHT- and vehicle-treated G_1 mice (Figures 3A and 3B). The more aggressive nature of 4-OHT-treated $G_{3\text{-}4}$ lymphomas was particularly evident from infiltration into brain (4/16) which was not

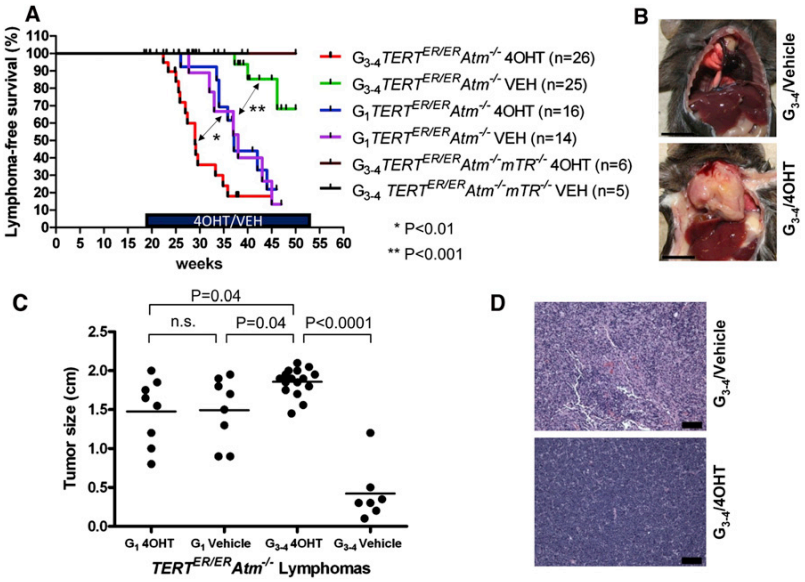

Figure 1. Telomerase Reactivation in Late-Generation *TERT*$^{ER/ER}$ *Atm*$^{-/-}$ Mice Promotes T Cell Lymphomagenesis

(A) Kaplan-Meier curves (Log-rank test) of T cell thymic lymphoma-free survival for G_1 and G_{3-4} *TERT*$^{ER/ER}$ *Atm*$^{-/-}$ (*mTR*$^{-/-}$) mice treated with 4-OHT or vehicle.

(B) Representative T cell thymic lymphoma of G_{3-4} *TERT*$^{ER/ER}$ *Atm*$^{-/-}$ mice treated with 4-OHT or vehicle. Scale bars represent 1 cm.

(C) Tumor sizes of G_1 and G_{3-4} *TERT*$^{ER/ER}$ *Atm*$^{-/-}$ lymphomas treated with 4-OHT or vehicle (t test, and error bars indicate SD).

(D) Representative images of H&E-stained G_{3-4} *TERT*$^{ER/ER}$ *Atm*$^{-/-}$ lymphomas treated with 4-OHT or vehicle. Scale bars represent 100 μm.

See also Figure S1.

observed in G_1 necropsies (n = 16) (Figures 3A and 3B), demonstrating that the malignant progression of initiated tumors is enabled by somatic reactivation of telomerase. This acquisition of more aggressive tendencies may stem in part from increased genome instability during the formative stages of tumor development prior to telomerase activation. Indeed, telomere dysfunction-induced bridge-fusion-breakage events can generate non-reciprocal translocations as well as regional amplifications and deletions at sites of breakage that, under biological selection, can result in cancer-promoting copy number changes (Artandi et al., 2000; Maser et al., 2007; O'Hagan et al., 2002). To examine this possibility, we compared cytogenetic and genomic profiles of 4-OHT-treated G_{3-4} tumors and 4-OHT-treated G_1 tumors, the latter without a period of telomere-driven crisis. Consistent with previous work (Maser et al., 2007), spectral karyotype (SKY) analysis showed a 3-fold increase in chromosomal rearrangements including nonreciprocal translocations in 4-OHT-treated G_{3-4} tumors (n = 3) relative to 4-OHT-treated G_1 tumors (n = 3) (Figures 3C and 3D, 25.8 versus 8.8 total NRTs per metaphase, respectively; $p < 0.0001$). The baseline of 8.8 NRTs per metaphase is consistent with previous work that ATM deficient tumors experience increased DNA double-stranded breaks, which promote chromosomal rearrangements as well (Xu et al., 1996).

Examination of copy number alterations (CNAs) in 18 G_{3-4}-4-OHT, 10 G_1-4-OHT, and 5 G_{3-4}-VEH tumors (Figure 3E; Figures S3A and S3B) revealed novel copy number gains on chromosomes 12, 17, and 18 and copy number losses on chromosome 14 in G_{3-4}-4-OHT tumors but not G_1-4-OHT tumors, consistent with increased genomic instability in late-generation tumors (Figure 3E; Figure S3A). Notably, G_{3-4}-4-OHT and G_{3-4}-VEH tumors show comparable levels of clonal CNAs, consistent with the view that wholesale genomic events driving lymphomagenesis occurs early in cancer development and that telomerase reactivation does not discernibly alter the scope of clonal genomic events in these cancers (Figure 3E; Figure S3B). Along these lines, we assessed whether the observed CNAs in G_{3-4}-4-OHT mice might contribute to the lymphomagenesis by examining whether murine and human lymphomas sustain orthologous CNA events than might be expected by chance as conducted previously (Maser et al., 2007). Array-CGH profiles of G_{3-4}-4-OHT tumors identified 4,928 genes resident within regions of genomic gain and 2,297 genes resident within regions of genomic loss with the use of Segment Gain or Loss (SGOL) algorithm (Wiedemeyer et al., 2010; Extended Experimental Procedures). Comparison of G_{3-4}-4-OHT tumors to human T-ALLs (Maser et al., 2007) showed that 565 of 4,928 amplified genes (11.5%) and 300 of 2,297 deleted genes (13%) are targeted for copy number alteration in both species (Table S1), which are significantly higher than those expected by chance (n = 10,000; p = 3e-04 and 2e-04 for amplification and deletion, respectively) (Figure S3C). These cross-species shared copy number altered genes include several known tumor suppressors and oncogenes implicated in T-ALL biology such as Crebbp, Ikaros, Abl, Notch1, Myc, and PTEN (Figure 3E). These data and previous work (Maser et al., 2007; O'Hagan et al., 2002) suggest that telomere dysfunction provides a mechanism that promotes structural genome alterations of cancer-relevant loci, which not only drive primary tumorigenesis but also confer additional malignant properties such as enhanced invasiveness.

Genetic Extinction of Telomerase Inhibits Cancer Growth and Leads to Eventual Tumor Re-Emergence

The *TERT-ER* system affords exploration of the impact of genetic extinction of telomerase activity in established cancers that, similar to human cancers, had evolved to first experience telomere dysfunction, and then subsequently acquire telomerase activity. In particular, this genetic model system enables assessment of tumor biological impact and potential adaptive mechanisms of antitelomerase therapy following reacquisition of telomere dysfunction. Freshly harvested 4-OHT-treated G_{3-4} tumor cells mice were passaged directly through SCID mice

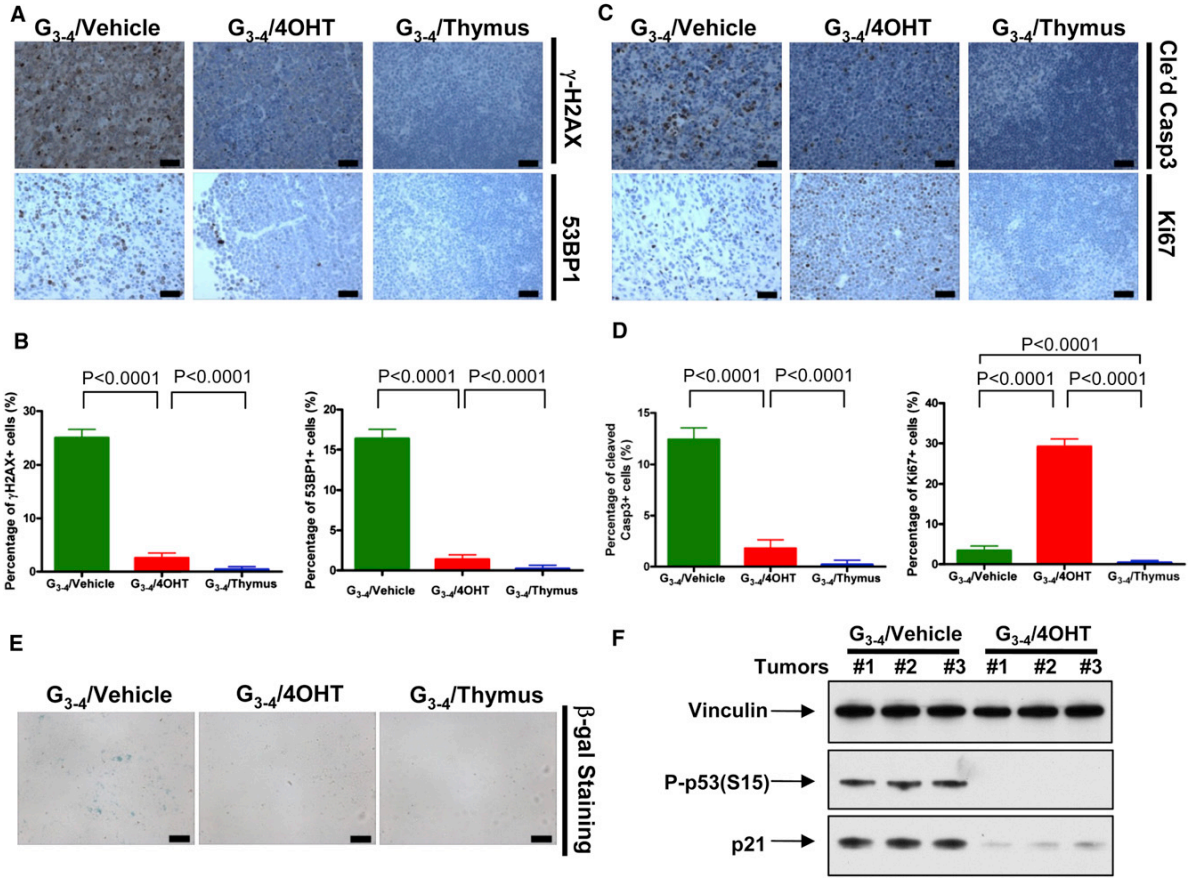

Figure 2. Telomerase Reactivation Alleviates Telomere Dysfunction and Checkpoints in Late-Generation *TERT*$^{ER/ER}$ *Atm*$^{-/-}$ Lymphomas

(A) Representative immunohistochemistry staining of γ-H2AX and 53BP1 in G_{3-4} *TERT*$^{ER/ER}$ *Atm*$^{-/-}$ thymus and lymphomas treated with 4-OHT or vehicle.

(B) Quantification of (A) (n = 5, t test).

(C) Representative immunohistochemistry staining of cleaved Caspase 3 and Ki67 in G_{3-4} *TERT*$^{ER/ER}$ *Atm*$^{-/-}$ thymus and lymphomas treated with 4-OHT or vehicle.

(D) Quantification of (C) (n = 5, t test).

(E) Representative beta-gal staining of G_{3-4} *TERT*$^{ER/ER}$ *Atm*$^{-/-}$ thymus and lymphomas treated with 4-OHT or vehicle (n = 3).

(F) Immunoblotting of phosphorylated p53 (S15) and p21 in G_{3-4} *TERT*$^{ER/ER}$ *Atm*$^{-/-}$ thymus and lymphomas treated with 4-OHT or vehicle.

Error bars indicate SD and scale bars represent 100 μm.

See also Figure S2.

preimplanted with vehicle or 4-OHT tablets (Figure S4A). Of 15 primary tumors lines (ten mice per each passage of treatment; 10^7 cells per intraperitoneal injection), 11 lines generated xenograft tumors. In first and second passages (P_1 and P_2), these lines showed no differences in the two treatment arms in terms of penetrance and latency (Figure 4A; P_1 and P_2). However, at third passage (P_3), 9 of 11 lines showed lower penetrance and longer latency in the vehicle-treated arm relative to the 4-OHT-treated arm, a profile consistent with the view that multiple rounds of cell division are needed to achieve sufficient telomere erosion and re-entry into crisis. Six of these nine lines showed complete loss of tumor formation in the vehicle-treated arm, whereas three lines yielded escaping tumors in several vehicle-treated recipient mice (Figure 4A; P_3). When these escaping P_3 tumors were passaged to P_4, they reacquired aggressive malignant properties approaching those of matched 4-OHT controls (Figure 4A; P_4), suggesting acquisition of resistant mechanisms to counteract telomerase deficiency. Moreover, 2 of the original 11 tumor lines did not show any attenuation of tumor growth in the vehicle-treated arm compared with the 4-OHT-treated arm (data not shown), suggesting early acquisition of such resistant mechanisms (see below).

To assess how G_{3-4}-4-OHT tumors respond to telomerase extinction on molecular level, we audited p53 signaling, DNA damage foci and apoptosis in serial passages of the two treatment arms. In 4-OHT-treated P_1 to P_4 and vehicle-treated P_1 tumor cells, p53 signaling, DNA damage foci and apoptosis levels were similar to those of parental tumor cells

A

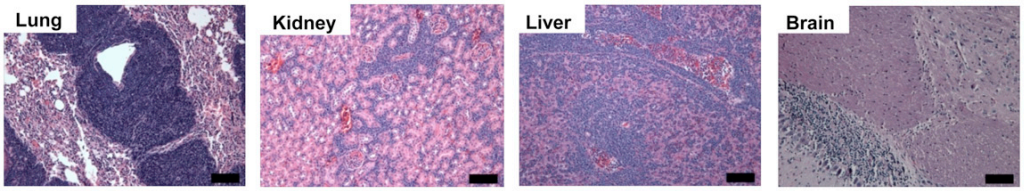

B

Genotype \ Tissue	Lymph node/Spleen	Lung	Kidney	Liver	Bone marrow	Brain
G_{3-4} $TERT^{ER/ER}Atm^{-/-}$4OHT	10/16	8/16	8/16	7/16	6/16	4/16
G_{3-4} $TERT^{ER/ER}Atm^{-/-}$VEH	0/7	0/7	0/7	0/7	0/7	0/7
G_1 $TERT^{ER/ER}Atm^{-/-}$4OHT+VEH	4/16	2/16	2/16	2/16	2/16	0/16

C

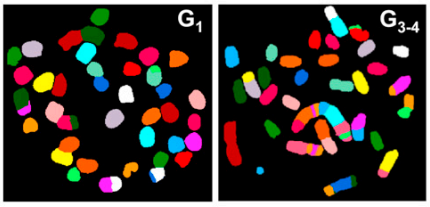

D

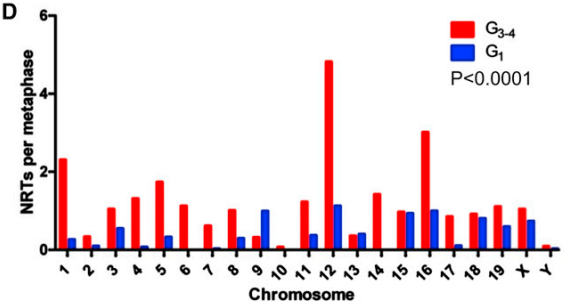

E

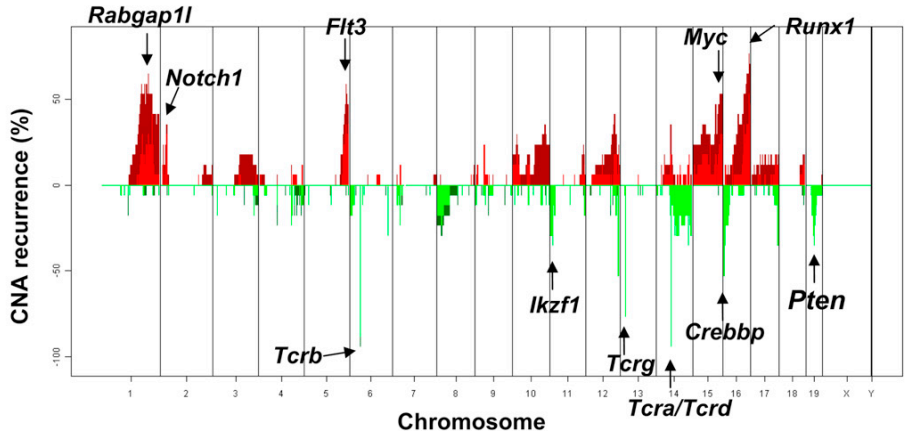

Figure 3. Telomerase Reactivation Promotes Invasiveness of Late-Generation $TERT^{ER/ER}$ $Atm^{-/-}$ Lymphomas

(A) Representative images of infiltrated organs (lung, kidney, liver, and brain) in G_{3-4} $TERT^{ER/ER}$ $Atm^{-/-}$ mice treated with 4-OHT. Scale bars represent 100 μm.

(B) Quantification of infiltrating incidence of G_1 and G_{3-4} $TERT^{ER/ER}$ $Atm^{-/-}$ mice treated with 4-OHT or vehicle.

(C) Representative spectral karyotype (SKY) images from metaphases of G_1 and G_{3-4} $TERT^{ER/ER}$ $Atm^{-/-}$ lymphomas treated with 4-OHT.

(D) Quantification of nonreciprocal translocations (NRTs) detected by SKY in G_1 (n = 3) and G_{3-4} (n = 3) $TERT^{ER/ER}$ $Atm^{-/-}$ lymphomas treated with 4-OHT ($p < 0.0001$, t test).

(E) Recurrence plot of CNAs defined by array-CGH for 18 G_{3-4}-4-OHT lymphomas. The *x* axis shows the physical location of each chromosome. The percentage of tumors harboring gains (dark red, $\log_2 \geq 0.3$), amplifications (bright red, $\log_2 \geq 0.6$), losses (green, $\log_2 \leq -0.3$), and deletions (dark green, $\log_2 \leq -0.6$) for each locus is depicted. Locations of physiologically relevant CNAs of TCR loci and some known cancer genes are indicated with asterisks.

See also Figure S3 and Table S1.

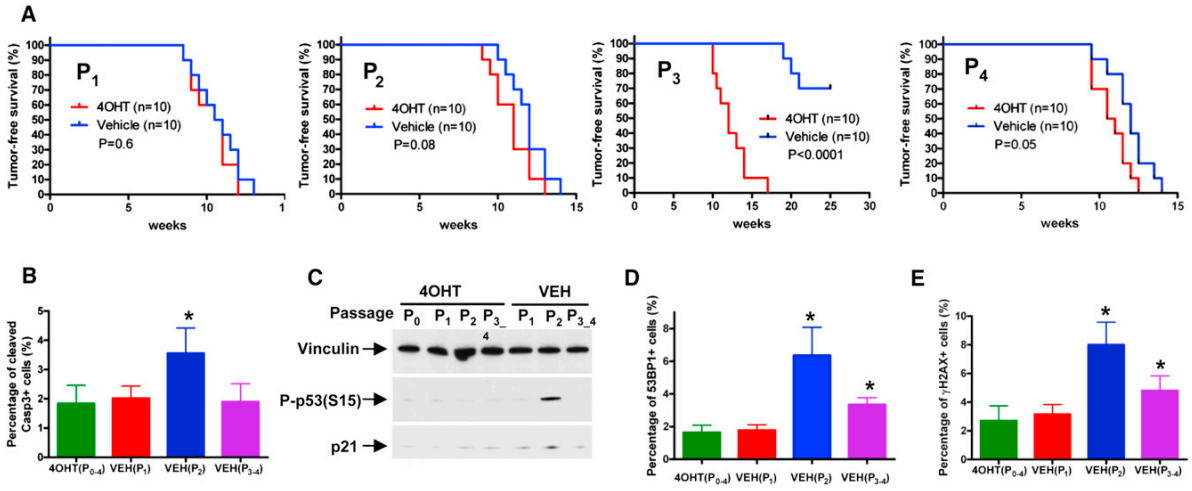

Figure 4. Telomerase Depletion in Late-Generation 4-OHT-*TERT*$^{ER/ER}$ *Atm*$^{-/-}$ Lymphomas Leads to Cell Death and Resistance

(A) Kaplan-Meier curves (Log-rank test) of lymphoma-free survival of 4OHT- or vehicle- treated mice serially transplanted with G_{3-4} *TERT*$^{ER/ER}$ *Atm*$^{-/-}$ lymphomas.
(B) Quantification of cleaved Caspase 3 positive cells in serially transplanted lymphomas treated with 4OHT or vehicle (n = 3–5, t test).
(C) Immunoblotting of phosphorylated p53 (S15) and p21 in serially transplanted lymphomas treated with 4OHT or vehicle.
(D) Quantification of 53BP1 foci positive cells in serially transplanted lymphomas treated with 4OHT or vehicle (n = 3–5, t test).
(E) Quantification of γ-H2AX foci positive cells in serially transplanted lymphomas treated with 4OHT or vehicle (n = 3–5, t test).
Error bars indicate SD (*p < 0.01 relative to any other individual samples in the same group). See also Figure S4.

(P_0) (Figures 4B–4E). In contrast, vehicle-treated P_2 tumor cells showed significantly higher levels of p53 signaling, DNA damage foci and apoptosis, and all of these processes were reduced in the resistant vehicle-treated P_{3-4} tumor cells (Figures 4B–4E), raising the possibility that these resistant tumors may have stabilized their telomeres to alleviate these checkpoints. Intriguingly, while DNA damage foci were reduced in the resistant tumors compared with the vehicle-treated P_2 tumors, these foci remain higher than telomerase+ (4-OHT-treated) tumors (Figures 4D and 4E), consistent with residual genotoxic stress in the resistant tumors. However, despite ongoing DNA damage signaling, apoptosis was not observed, which is consistent with compromised p53 signaling in the resistant tumors (Figure S4B).

Emergence of ALT in Tumors following Extinction of Telomerase

To elucidate adaptive mechanisms following telomerase extinction, we cataloged telomere lengths in serially passaged tumors in the two treatment arms. In passaged 4-OHT-treated P_1 to P_4 tumor cells, telomere lengths remained unchanged from those in parental tumor cells, while vehicle-treated P_1 and P_2 tumor cells showed progressive telomere shortening (Figure 5A). However, vehicle-treated P_{3-4} tumor cells showed a sharp increase in average and maximal telomere lengths that exceeded those in matched 4-OHT controls (Figure 5A); however, these vehicle-treated P_{3-4} tumor cells tumor cells showed more telomere signal-free ends by telomere-FISH (Figures 5B and 5C), a picture consistent with higher heterogeneity in the distribution of telomere lengths in resistant tumors. In addition, costaining of promyelocytic leukemia (PML) bodies and telomeres showed an increase in ALT-associated PML bodies (APBs) (Figures 5D and 5E), and telomere-FISH showed more extrachromosomal telomere fragments in the vehicle-treated P_{3-4} tumors cells relative to the matched 4-OHT controls (Figures 5F and 5G). Finally, vehicle-treated P_{3-4} tumor cells showed an increased telomere Sister Chromatid Exchange (tSCE) rate than matched 4-OHT controls (Figures 5H and 5I). These collective data provide clear evidence of ALT in vehicle-treated P_{3-4} tumor cells that have resumed robust tumor growth in vivo. In addition, the two tumor lines, which did not show any attenuation of tumor growth in the vehicle-treated arm, also showed ALT features including APBs and extra-chromosomal telomere fragments (Figures S5A and S5B), consistent with the early acquisition of ALT.

ALT Tumors Show Upregulation of a Master Regulator of Mitochondrial Biogenesis/Function and Oxidative Defense

Serial loss of telomere function and genome destabilization in this genetically defined system provided an unprecedented opportunity to discern on a genome scale the associated adaptive molecular events in these ALT+ tumor cells via integrated transcriptomic and aCGH profile analyses. Cluster analysis of transcriptomes of 4-OHT-treated P_4 tumors (n = 3), and parental 4-OHT-treated tumor revealed no significant differences (Figure 6A), consistent with genomic stability brought about by continuous telomerase activity. In contrast, vehicle-treated ALT+ P_4 tumor (n = 5) expression profiles showed significant differences relative to the 4-OHT-treated telomerase-positive P_4 tumors, 891 upregulated and 1,345 downregulated genes in ALT+ tumors with 1.5-fold change and $p < 0.01$ (t test; Figure 6A; Table S2). Pathway (IPA) analysis of the ALT-specific transcriptome showed strong representation of networks centering on

mitochondrial biology and oxidative stress regulation (Figure S6A). Consistent with the known role of DNA recombination in ALT (Fan et al., 2009; Zhong et al., 2007), MRE11 and FANCA were also upregulated in these ALT+ tumors (Figures S6B and S6C). With regard to mitochondria and oxidative pathways, Q-PCR verified aberrant expression of several key genes in these networks including upregulation of a master regulator of mitochondrial biology and oxidative defense, PGC-1β, and its targets such as NRF2, SOD2, and Catalase, among others (Figure 6B).

As noted, telomere dysfunction-induced DNA double-strand breakage process and biological selection can lead to functionally relevant CNAs, prompting us to identify potential genetic events that may inform how ALT+ cells cope with telomere-based crisis. To that end, we performed array-based comparative genomic hybridization (aCGH) analysis of ALT+ versus telomerase+ P_4 tumors from the two treatment arms. While serially transplanted telomerase+ tumors showed minimal CNA differences relative to the parental tumor, ALT+ tumors acquired numerous CNAs (see below). Strikingly, integrated transcriptomic and copy number analysis revealed PGC-1β as the only gene in the mitochondrial function and oxidative stress regulation pathways showing both upregulated expression and copy number gain in the ALT+ tumors relative to telomerase+ tumors (Table S3); these genomic data raised the possibility that PGC-1β might be a major driver of the adaptive response to telomere dysfunction.

To ask whether PGC-1β amplification/overexpression is a common event in our ALT+ tumors, we profiled eight independent telomerase+ tumors and five independent ALT+ tumors, and found that three of five ALT+ tumors (60%) show amplification of a large region of chromosome 18, which includes PGC-1β gene, whereas none of the telomerase+ tumors (n = 8) sustain such genomic alterations (Figure 6C). To reinforce the potential role of PGC-1β upregulation as a possible adaptive response to ALT, we examined PGC-1β expression levels in ALT+ tumors without PGC-1β amplification, and established that PGC-1β expression is significantly higher in ALT+ tumors than their corresponding telomerase+ tumors (Figure S6D).

ALT+ Tumors Have Higher Levels of Mitochondrial Dysfunction and Reactive Oxygen Species Relative to Telomerase+ Tumors

PGC-1α and PGC-1β are master regulators of mitochondrial biogenesis and function, play integral roles in the regulation of genes governing reactive oxygen species (ROS) defense, and are downregulated in normal tissues experiencing telomere dysfunction as a result of activated p53-mediated repression (Sahin et al., 2011). This framework, coupled with above genomic observations, prompted us to hypothesize that telomerase extinction and ensuing telomere dysfunction repress the mitochondrial biogenesis and function in cancer cells, and the adaptive response to such telomere-based crises targets the p53-PGC axis in an effort to restore the mitochondrial function. To assess this possibility, we assessed PGC network expression, mitochondrial mass and mitochondrial function in passaged 4-OHT-treated and vehicle-treated P_1-P_4 tumor cells. Mitochondria DNA content were maintained in the telomerase+ arm but sharply reduced in the vehicle-treated P_2 tumor cells yet significantly restored in the ALT+ $P_{3\text{-}4}$ tumor cells (Figure 6D). Correspondingly, in contrast to the telomerase+ arm or early passage of vehicle-treated tumor cells, vehicle-treated P_2 tumor cells showed reduced expression of PGC-1β and its major targets NRF-1, ERRα, PPARα, and TFAM which are critical for mitochondrial biogenesis and function (Figure 6E; note: PGC-1α is not expressed in these murine T cell lymphomas). These expression patterns were significantly normalized in the ALT+ $P_{3\text{-}4}$ tumor cells (Figure 6E).

With regard to mitochondrial function, mitochondrial respiration assays (normalized for mtDNA content) showed that vehicle-treated P_2 tumor cells have dramatically impaired mitochondrial respiration relative to telomerase+ cells (Figure 6F). ALT+ $P_{3\text{-}4}$ tumor cells show substantial improvement in mitochondrial respiration, although function remains somewhat compromised relative to those of telomerase+ cells (Figure 6F; Figure S6E). Finally, the capacity of PGC-1β to regulate oxidative defense genes (St-Pierre et al., 2006) and the integral role of mitochondria in ROS control (Murphy, 2009) prompted examination of intracellular ROS levels in ALT+ and telomerase+ tumor cells. Using the fluorescent dye DCF-DA protocol, FACS analysis showed significantly increased ROS levels in vehicle-treated P_2 tumor cells relative to 4-OHT-treated P_0 to P_4 and vehicle-treated P_1 tumor cells (Figure 6G; Figure S6F). In ALT+ tumor cells, ROS levels are lower than vehicle-treated P_2 tumor cells, albeit higher than telomerase+ tumor cell controls (Figure 6G; Figure S6F). Thus, telomere dysfunction in cancer cells is commonly associated with repression of PGC1β and its network resulting in mitochondrial mass decline and the adaptive responses to telomere dysfunction appear to involve not only activation of ALT telomere maintenance mechanism but also upregulation of genetic pathways promoting partial restoration of mitochondrial mass and function. Importantly, however, relative to telomerase+ cells, ALT+ tumor cells still have modestly elevated mitochondrial dysfunction and ROS which may reflect ongoing genotoxic stress relating to inefficiencies of telomere maintenance via ALT as reflected by moderately increased DNA damage foci above baseline in these tumors (see Figures 4D and 4E above).

ALT+ Tumors Show Increased Sensitivity to Inhibition of PGC-1β or SOD2

Because relatively functional mitochondria and moderate levels of ROS are required for cancer cell survival (Weinberg et al., 2010), we asked whether shRNA-mediated knockdown of PGC-1β would have a negative or differential impact on telomerase+ and ALT+ tumor cells. Multiple independent shRNAs achieved PGC-1β knockdown in both telomerase+ and ALT+ tumor cells (Figure 7A). Consistent with the pivotal role of PGC coactivators in mitochondrial function and ROS regulation, both telomerase+ and ALT+ tumor cells showed significantly reduced mitochondrial numbers, compromised mitochondrial function, and increased ROS after PGC-1β knockdown (Figures 7B–7D). Notably, ALT+ tumor cells showed greater compromise in all three categories relative to telomerase+ tumor cells (Figures 7B–7D), raising the possibility that ALT+ tumor cells may show greater sensitivity to PGC-1β inhibition with increased mitochondrial dysfunction and ROS toxicity. Correspondingly,

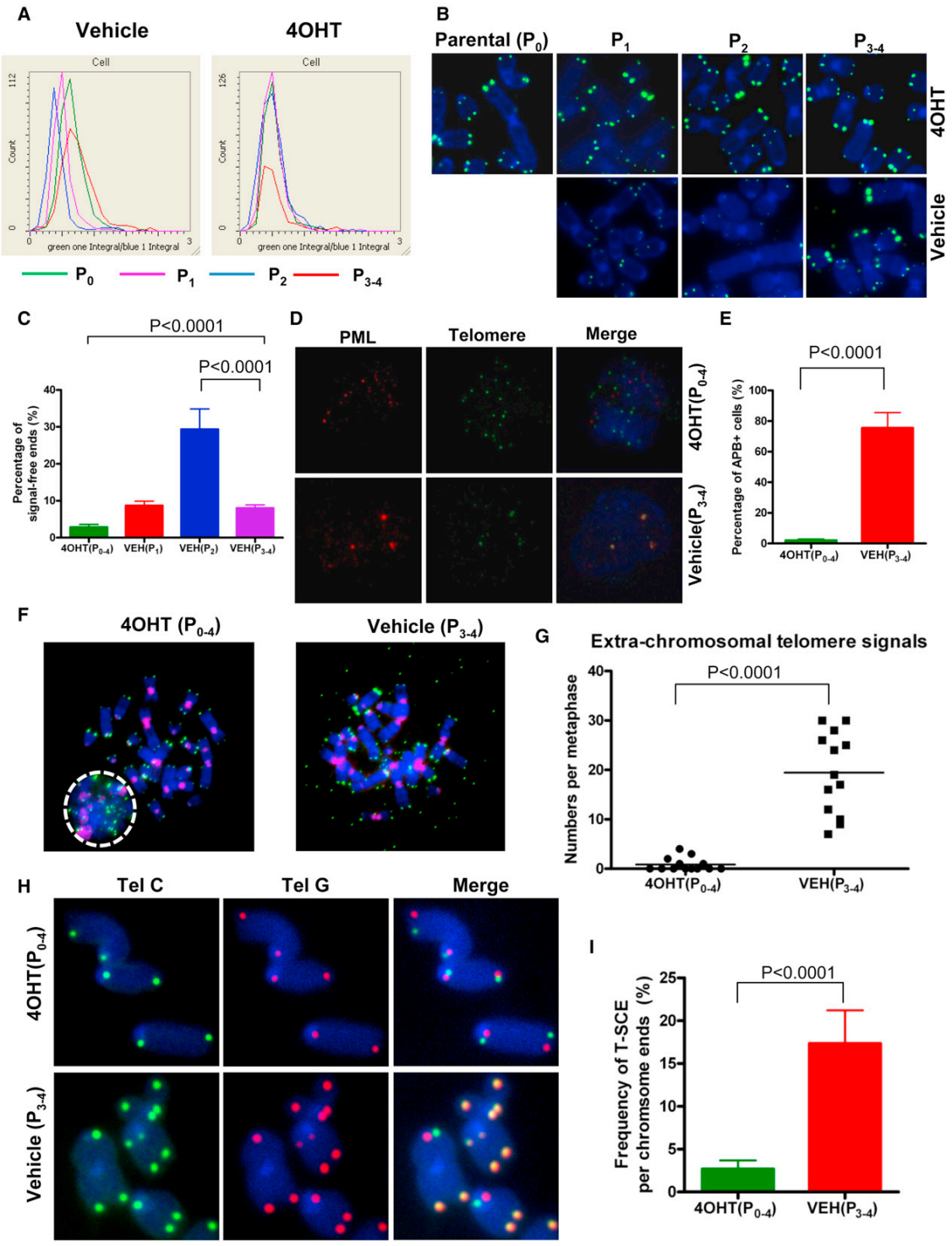

Figure 5. *TERT*$^{ER/ER}$ *Atm*$^{-/-}$ Lymphomas Developed ALT in the Absence of Telomerase

(A) Telomere lengths of serially transplanted lymphomas treated with 4OHT or vehicle measured by telomere-FISH coupled laser scanning cytometry (n = 3–5).

(B) Telomere signal-free ends were measured by telomere-FISH in serially transplanted lymphomas treated with 4OHT or vehicle.

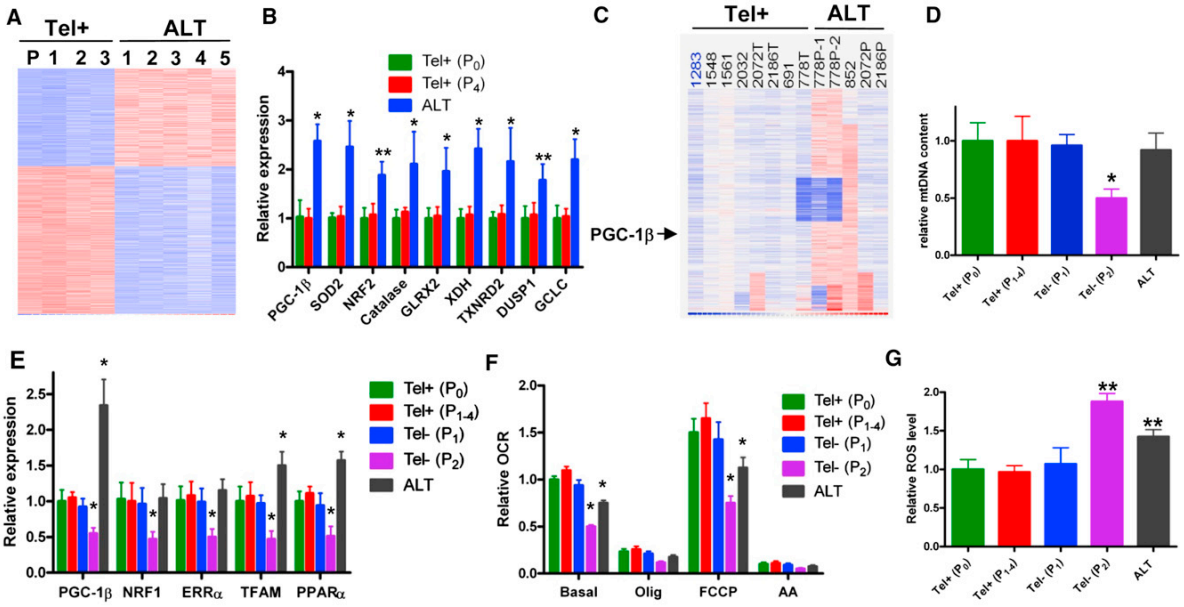

Figure 6. ALT+ Tumors Overcome Their Higher Levels of ROS and Mitochondrial Dysfunction by Upregulating PGC-1β and Other Oxidative Defense Genes

(A) Microarray heat map of differentially expressed genes in ALT+ tumors relative to telomerase+ lymphomas.
(B) RT-qPCR validation of oxidative defense genes upregulated in ALT+ lymphomas (n = 3, t test).
(C) CNVs of chromosome 18 in eight independent telomerase+ lymphomas and five independent ALT+ lymphomas.
(D) Mitochondria DNA contents of serially transplanted lymphomas and ALT+ lymphomas were measured by qPCR (n = 3–5, t test).
(E) RT-qPCR validation of mitochondrial biogenesis genes in serially transplanted lymphomas and ALT+ lymphomas (n = 3, t test).
(F) Oxygen Consumption Rates (OCRs) relative to mtDNA contents were measured in serially transplanted lymphomas and ALT+ lymphomas (n = 3, t test).
(G) ROS levels of serially transplanted lymphomas and ALT+ lymphomas were measured by DCFDA staining (n = 3-5, t test).
Error bars indicate SD (*p < 0.001, **p < 0.01 relative to any other individual samples in the same group). See also Figure S6 and Tables S2 and S3.

shRNA-mediated knockdown of PGC-1β showed a minimal impact on telomerase+ tumor growth and a profound impact on ALT+ cells (Figure 7E; median survival from 15 weeks to 19 weeks versus 17 weeks to over 30 weeks; p = 0.0065, Cox model). These findings are consistent with increased apoptosis in ALT+ tumors with PGC-1β knockdown (Figure S7A). In addition, since SOD2 is a major ROS antioxidant in mitochondria, regulated by PGC-1β, and highly expressed in ALT+ cells (Figure 6B), we tested the impact of SOD2 knockdown in ALT+ and telomerase+ cells. As expected, SOD2 knockdown increased ROS levels in both telomerase+ and ALT+ cells, although ROS levels in ALT+ cells (both basal or after SOD2 knockdown) were substantially higher than those in telomerase+ cells (Figures 7F and 7G). On the biological level, while non-targeting shRNA-transduced telomerase+ and ALT+ cells showed similar cell survival rates (MTT assay), SOD2 knockdown in ALT+ cell decreased survival greater than in telomerase+ cells (Figure 7H; p = 0.02), suggesting that ALT+ cells are more sensitive to increase of ROS than telomerase+ cells. The sensitivity of ALT+ cells to ROS was further confirmed by NAC rescue experiments on ALT+ cells with PGC-1β and SOD2 knockdown (Figures S7B and S7C). Together, these data suggest that targeting PGC or ROS detoxifying genes may enhance the therapeutic impact of antitelomerase therapy, particularly in the context of ALT+-resistant cells.

DISCUSSION

One of the hallmarks of cancer cells is the shift from mitochondrial to glycolytic metabolism as the prime source of energy

(C) Quantification of telomere signal-free ends in serially transplanted lymphomas treated with 4OHT or vehicle (n = 3–5, t test).
(D) Representative images of ALT-associated PML body (APB) costained with PML and telomere.
(E) Quantification of ALT-associated PML Body (APB) numbers in resistant lymphomas and matched 4-OHT controls (n = 5, t test).
(F) Representative images of extrachromosomal telomere fragments in resistant tumors. Circled area indicates metaphase spread not separated well.
(G) Quantification of extrachromosomal telomere fragments in resistant tumors and matched 4-OHT controls (n = 5, t test).
(H) Representative images of telomere Sister Chromatid Exchange (tSCE) in resistant tumors.
(I) Quantification of telomere Sister Chromatid Exchange (tSCE) in resistant tumors and matched 4-OHT controls (n = 5, t test).
Error bars indicate SD. See also Figure S5.

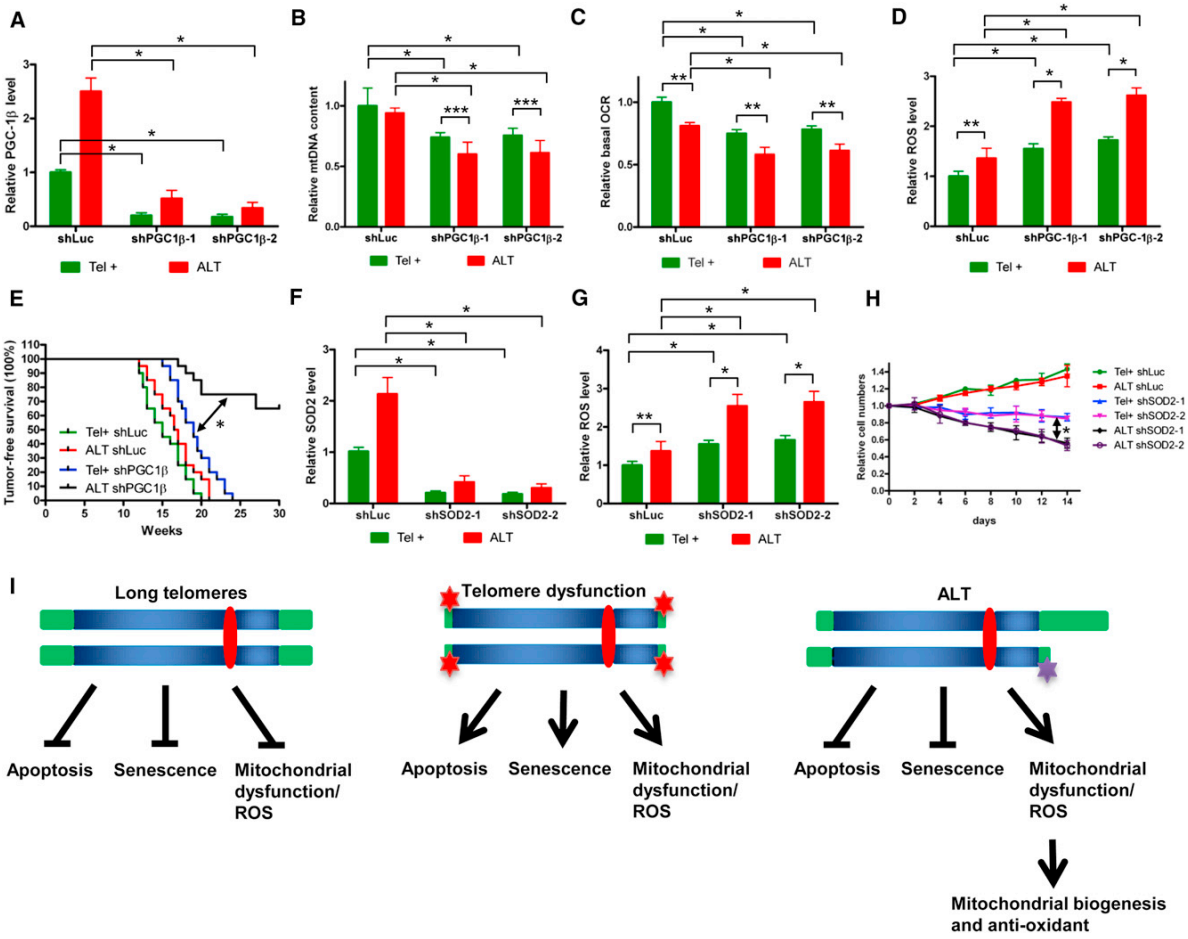

Figure 7. Inhibition of PGC-1β or SOD2 Differentially Kills ALT+ Tumors over Telomerase+ Tumors

(A) PGC-1β expression levels in telomerase+ and ALT+ tumor cells with PGC-1β shRNAs or control shRNA (shLuc) (n = 3, t test).
(B) Mitochondria DNA contents in telomerase+ and ALT+ tumor cells with PGC-1β shRNAs or control shRNA (shLuc) (n = 3, t test).
(C) Basal oxygen consumption rates (OCR) in telomerase+ and ALT+ tumor cells with PGC-1β shRNAs or control shRNA (shLuc) (n = 3, t test).
(D) ROS levels in telomerase+ and ALT+ tumor cells with PGC-1β shRNAs or control shRNA (shLuc) (n = 3, t test).
(E) Kaplan-Meier curves (Cox model test, p = 0.0065) of lymphoma-free survival of mice transplanted with telomerase+ and ALT+ tumor cells with PGC-1β shRNAs (shPGC-1β-1+ shPGC-1β-2) or control shRNA (shLuc).
(F) SOD2 expression levels in telomerase+ and ALT+ tumor cells with SOD2 shRNAs or control shRNA (shLuc) (n = 3, t test).
(G) ROS levels in telomerase+ and ALT+ tumor cells with SOD2 shRNAs or control shRNA (shLuc) (n = 3, t test).
(H) Relative cells numbers of telomerase+ and ALT+ tumor cells with SOD2 shRNAs or control shRNA (shLuc) (n = 3, two-way ANOVA, p = 0.02).
(I) Model of regulation of apoptosis, senescence and mitochondrial function in telomerase+, ALT+, and telomere-dysfunctional cells.
Error bars indicate SD (*p < 0.0001, **p < 0.001, ***p < 0.02, unless otherwise stated). See also Figure S7.

and anabolic support (Vander Heiden et al., 2009; Warburg, 1956). While this bioenergetic shift conveys decreased reliance on mitochondria as a major energy source for cancer cells, our genetic studies indicate a continued vital role in the maintenance of mitochondrial function in cancer. This view aligns with multiple lines of evidence suggesting that mitochondrial competence is indeed important for cancer cell viability (Jose et al., 2011; Koppenol et al., 2011) and efficient oncogene-mediated transformation (Gao et al., 2009; Weinberg et al., 2010; Wise et al., 2008; Yuneva et al., 2007). More specifically, our study uncovers a critical role of robust mitochondrial function in cancer cells, particularly for those cancer cells with ALT-maintained telomeres.

Why might ALT+ cancer cells exhibit exquisite sensitivity to inhibition of PGC expression or antioxidant defense? We speculate that continued DNA damage signaling at ALT-maintained telomeres perhaps due to altered chromatin (Heaphy et al., 2011) or inefficient capping via this mechanism could lead to mitochondrial damage. Mitochondria are the major intracellular source of ROS in mammalian cells, and dysfunctional mitochondria produce more ROS, which at excessively high levels is

known to be detrimental to cell survival (Lin and Beal, 2006; Murphy, 2009; St-Pierre et al., 2006). In this context, we propose that the pressure to maintain mitochondrial function reflects the need to maintain tolerable intracellular ROS levels. This oxidative defense mechanism may be particularly important for telomeres as ROS are particularly injurious toward the G-rich sequences of telomeres (Hall et al., 1996; Oexle and Zwirner, 1997; Retèl et al., 1993), thereby causing increased telomere dysfunction in the absence of efficient telomerase-mediated repair. Correspondingly, our combined genomic and functional studies establish that ALT+ cells strive to maintain adequate mitochondrial and oxidative defense functions and show exquisite sensitivity to loss of such function. On the molecular level, this work also establishes that the intimate PGC-directed link between telomeres and mitochondria identified recently in normal tissues (Sahin et al., 2011) is operative in cancer cells (Figure 7I).

About 15% of human cancers maintain their telomeres in the absence of telomerase activity by the ALT mechanism. The existence of a telomerase-independent telomere maintenance mechanism was first identified in yeast with telomerase deficiency, and this mechanism was demonstrated to be dependent on *RAD52*, a gene involved in homologous recombination (Lundblad and Blackburn, 1993). Subsequent studies established that the ALT mechanism in human cancer cells requires certain DNA recombination proteins, including the MRN complex (MRE11, RAD50, and NBS1) (Jiang et al., 2005; Zhong et al., 2007), SMC5-SMC6 complex (Potts and Yu, 2007), flap endonuclease 1 (FEN1) (Saharia and Stewart, 2009), MUS81 (Zeng et al., 2009), Fanconi anemia group D2 (FANCD2), and Fanconi anemia group A (FANCA) (Fan et al., 2009). In our model, *MRE11* and *FANCA* genes are indeed upregulated in ALT+ cells relative to telomerase+ cells (Figures S4B and S4C). These observations provide genetic evidence in mammalian cells of the importance of these factors for DNA recombination-dependent ALT mechanism in this cancer model.

Our studies also highlight that, while ALT+ cells suppress apoptosis and senescence as efficiently as telomerase+ cells, these cells do not fully restore mitochondrial function which we speculate may relate to ongoing genotoxic stress partly associated with less efficient telomere capping by ALT-mediated telomere maintenance (Cesare et al., 2009) as well as p53-independent repression of PGC (Sahin et al., 2011). In ALT+ cells, the importance of this mitochondrial maintenance program is underscored by the upregulated PGC network signaling on both the genomic (copy number) and transcriptional levels (Figure 7I). That the PGC network is a vital regulator in our ALT+-resistant tumors is further substantiated by our analysis of published transcriptomic data comparing human ALT+ with telomerase+ osteosarcomas (Lafferty-Whyte et al., 2009). Specifically, comparison of three key network genes (PGC-1α, NRF2, and SOD2; PGC-1β data is not available in this data set) in ten ALT+ and eight telomerase+ osteosarcomas showed that five of ten ALT+ osteosarcomas have significantly higher levels of one or multiple of PGC-1α, NRF2, and SOD2 genes relative to the basal levels, which is more prominent than telomerase+ tumors (Figure S6G) ($p = 0.04$), suggesting that upregulation of mitochondrial function and ROS defense pathway genes is important in other ALT+ cancer types. Thus, our genetic modeling of telomerase extinction in cancer increases our understanding of how tumor cells might respond and adapt to telomerase inhibition and illuminates a clinical path hypothesis utilizing combination regimens targeting telomerase and PGC-mediated adaptive mechanisms in cancer.

EXPERIMENTAL PROCEDURES

Mice

Atm, *Terc*, and *TERT-ER* mice described previously (Jaskelioff et al., 2011; Maser et al., 2007; Wong et al., 2003) were interbred and backcrossed to high grade of C57BL/6 (over 95%). The mating strategy to obtain experimental cohorts G_0, G_1, and G_{3-4} is shown in Figure S1A. 4-OHT time release pellets (5 mg; Innovative Research of America) were inserted subcutaneously at age of 18 weeks to reach steady-state blood levels of 1 ng ml^{-1} 4-OHT for 60 consecutive days.

Histology, Tumor Characterization, and Sample Preparation

Antibodies used for IHC include anti-Ki67 (Dako), anti-53BP1 (Bethyl Labs), anti-γH2AX (Bethyl Labs), and anti-Cleaved Caspase 3 (Cell Signaling). For FACS analysis, cells were immunostained with CD4, CD8, and CD3 antibodies (eBioscience) and analyzed on a BD FACSCanto II (BD Biosciences).

Cytogenetic Analysis

For metaphase preparation, metaphases were obtained from colcemid-treated cells incubated in 105 mM KCl hypotonic buffer for 15 min before fixation in 3:1 methanol–acetic acid. Spectral karyotyping (SKY) was done using the SkyPaint Kit and SkyView analytical software (Applied Spectral Imaging) according to manufacturer's protocols. For telomere-FISH (fluorescent in situ hybridization), metaphase spreads were applied with telomere-specific T_2AG_3-FITC PNA (peptide nucleic acid) probes and centromere-specific Cent-Cy3 or Cent-pacific blue PNA probes, and counter-stained with DAPI (for microscopy) or TOTO3 (for laser scanning). Laser scanning cytometry quantification was performed with an iCys Research Imaging Cytometer (Compucyte) as described earlier (Jaskelioff et al., 2011; Sahin et al., 2011).

Telomere Sister Chromatid Exchange Assay

Telomere Co-FISH staining was performed as previously described (Potts and Yu, 2007). Details are described in Extended Experimental Procedures.

RT-qPCR, Mitochondria DNA Content Measurement, and Western Blot

RT-qPCR primers are described in Table S4. Mitochondrial DNA content was measured by the relative levels of CoxI versus beta globin by qPCR. CoxI and beta globin primers are described in Table S4. Antibodies used for Western blotting are anti-phospho p53 (ser15, Cell Signaling), anti-p21 (Santa Cruz Biotechnology), anti-Vinculin (Sigma), and anti-Mre11 (BD Biosciences).

shRNA Knockdown

Lentiviral based shRNA constructs targeting mouse PGC-1β and SOD2 were ordered from The Dana-Farber/Harvard Cancer Center DNA Resource Core. Verified shRNA sequences were cloned into inducible lentiviral constructs PLKO-TRC-901 (IPTG inducible; Broad Institute) and PLKO-Tet (Doxycycline inducible; Novartis).

Pathway Analysis

Eight hundred ninety-one upregulated and 1,345 downregulated genes with 1.5-fold change and $p < 0.01$ in ALT+ tumors relative to telomerase+ tumors were applied with Knowledge-based Pathway (IPA) analysis. The significantly represented pathways were compared with the pathways obtained from the similar analysis on ten ALT+ and eight telomerase+ osteosarcomas (Lafferty-Whyte et al., 2009). Overlapped pathways are listed.

Array-CGH Profiling and Analyses

Array-CGH, SGOL score analysis, homologous mapping, and permutation analysis are described in Extended Experimental Procedures.

Mitochondrial Oxygen Consumption Measurements in Live Cells

Oxygen consumption rates (OCRs) were measured using the Seahorse XF24 instrument (Seahorse Biosciences). Basal mitochondrial respiration were measured at four time points, and respiration nonlinked to mitochondrial ATP synthesis were measured at four time points after adding 1 μM oligomycin. Nonmitochondrial OCRs were obtained by adding 5 μM antimycin A, and uncoupled respiration was obtained by adding 1 μM FCCP.

ROS Measurement

For determination of ROS levels, tumor cells were stained with 5 μM CM-H_2 DFCDA (Invitrogen) at 37°C for 30 min, followed by FACS analysis on a BD FACSCanto II (BD Biosciences).

COX Model Test

Effects of shPGC-1β knockdown on Tel+ and ALT+ cells were tested by Cox analysis. Details are described in Extended Experimental Procedures.

ACCESSION NUMBERS

Microarray (GSE35044) and aCGH (GSE35045) data were deposited in GEO (http://www.ncbi.nlm.nih.gov/geo/) under the accession numbers indicated.

SUPPLEMENTAL INFORMATION

Supplemental Information includes Extended Experimental Procedures, seven figures, and four tables and can be found with this article online at doi:10.1016/j.cell.2011.12.028.

ACKNOWLEDGMENTS

We thank S. Jiang, R. Narurkar, and E. Fletcher-Sananikone for excellent mouse husbandry and care, and all members of DePinho and Chin labs for helpful discussion. We also thank Yingchui Liu for the Cox model analysis. J.H. and B.G. were supported by the leukemia and lymphoma society fellowship. A.T.B. is supported by the Helen Hay Whitney fellowship. M.L. is supported by the Fundación Ramón Areces fellowship. O.S.S. is supported by R01 (R01-DK074778 and R01-DK56690) grants from NIH. L.C. and R.A.D. are supported by R01 (R01CA84628) and U01 (U01CA141508) grants from NIH. R.A.D. is an Ellison Foundation for Medical Research Senior Scholar and an American Cancer Society Research Professor.

Received: August 27, 2011
Revised: November 8, 2011
Accepted: December 30, 2011
Published: February 16, 2012

REFERENCES

Agrawal, A., Dang, S., and Gabrani, R. (2012). Recent patents on anti-telomerase cancer therapy. Recent Patents Anticancer. Drug Discov. *7*, 102–117.

Artandi, S.E., and DePinho, R.A. (2010). Telomeres and telomerase in cancer. Carcinogenesis *31*, 9–18.

Artandi, S.E., Chang, S., Lee, S.L., Alson, S., Gottlieb, G.J., Chin, L., and DePinho, R.A. (2000). Telomere dysfunction promotes non-reciprocal translocations and epithelial cancers in mice. Nature *406*, 641–645.

Begus-Nahrmann, Y., Lechel, A., Obenauf, A.C., Nalapareddy, K., Peit, E., Hoffmann, E., Schlaudraff, F., Liss, B., Schirmacher, P., Kestler, H., et al. (2009). p53 deletion impairs clearance of chromosomal-instable stem cells in aging telomere-dysfunctional mice. Nat. Genet. *41*, 1138–1143.

Cesare, A.J., and Reddel, R.R. (2010). Alternative lengthening of telomeres: models, mechanisms and implications. Nat. Rev. Genet. *11*, 319–330.

Cesare, A.J., Kaul, Z., Cohen, S.B., Napier, C.E., Pickett, H.A., Neumann, A.A., and Reddel, R.R. (2009). Spontaneous occurrence of telomeric DNA damage response in the absence of chromosome fusions. Nat. Struct. Mol. Biol. *16*, 1244–1251.

Chang, S., Khoo, C.M., Naylor, M.L., Maser, R.S., and DePinho, R.A. (2003). Telomere-based crisis: functional differences between telomerase activation and ALT in tumor progression. Genes Dev. *17*, 88–100.

Chin, L., Artandi, S.E., Shen, Q., Tam, A., Lee, S.L., Gottlieb, G.J., Greider, C.W., and DePinho, R.A. (1999). p53 deficiency rescues the adverse effects of telomere loss and cooperates with telomere dysfunction to accelerate carcinogenesis. Cell *97*, 527–538.

d'Adda di Fagagna, F., Reaper, P.M., Clay-Farrace, L., Fiegler, H., Carr, P., Von Zglinicki, T., Saretzki, G., Carter, N.P., and Jackson, S.P. (2003). A DNA damage checkpoint response in telomere-initiated senescence. Nature *426*, 194–198.

Fan, Q., Zhang, F., Barrett, B., Ren, K., and Andreassen, P.R. (2009). A role for monoubiquitinated FANCD2 at telomeres in ALT cells. Nucleic Acids Res. *37*, 1740–1754.

Feng, J., Funk, W.D., Wang, S.S., Weinrich, S.L., Avilion, A.A., Chiu, C.P., Adams, R.R., Chang, E., Allsopp, R.C., Yu, J., et al. (1995). The RNA component of human telomerase. Science *269*, 1236–1241.

Gao, P., Tchernyshyov, I., Chang, T.C., Lee, Y.S., Kita, K., Ochi, T., Zeller, K.I., De Marzo, A.M., Van Eyk, J.E., Mendell, J.T., and Dang, C.V. (2009). c-Myc suppression of miR-23a/b enhances mitochondrial glutaminase expression and glutamine metabolism. Nature *458*, 762–765.

González-Suárez, E., Samper, E., Flores, J.M., and Blasco, M.A. (2000). Telomerase-deficient mice with short telomeres are resistant to skin tumorigenesis. Nat. Genet. *26*, 114–117.

Hall, D.B., Holmlin, R.E., and Barton, J.K. (1996). Oxidative DNA damage through long-range electron transfer. Nature *382*, 731–735.

Harley, C.B., and Sherwood, S.W. (1997). Telomerase, checkpoints and cancer. Cancer Surv. *29*, 263–284.

Heaphy, C.M., de Wilde, R.F., Jiao, Y., Klein, A.P., Edil, B.H., Shi, C., Bettegowda, C., Rodriguez, F.J., Eberhart, C.G., Hebbar, S., et al. (2011). Altered telomeres in tumors with ATRX and DAXX mutations. Science *333*, 425.

Jaskelioff, M., Muller, F.L., Paik, J.H., Thomas, E., Jiang, S., Adams, A.C., Sahin, E., Kost-Alimova, M., Protopopov, A., Cadiñanos, J., et al. (2011). Telomerase reactivation reverses tissue degeneration in aged telomerase-deficient mice. Nature *469*, 102–106.

Jiang, W.Q., Zhong, Z.H., Henson, J.D., Neumann, A.A., Chang, A.C., and Reddel, R.R. (2005). Suppression of alternative lengthening of telomeres by Sp100-mediated sequestration of the MRE11/RAD50/NBS1 complex. Mol. Cell. Biol. *25*, 2708–2721.

Jose, C., Bellance, N., and Rossignol, R. (2011). Choosing between glycolysis and oxidative phosphorylation: a tumor's dilemma? Biochim. Biophys. Acta *1807*, 552–561.

Karlseder, J., Broccoli, D., Dai, Y., Hardy, S., and de Lange, T. (1999). p53- and ATM-dependent apoptosis induced by telomeres lacking TRF2. Science *283*, 1321–1325.

Koppenol, W.H., Bounds, P.L., and Dang, C.V. (2011). Otto Warburg's contributions to current concepts of cancer metabolism. Nat. Rev. Cancer *11*, 325–337.

Lafferty-Whyte, K., Cairney, C.J., Will, M.B., Serakinci, N., Daidone, M.G., Zaffaroni, N., Bilsland, A., and Keith, W.N. (2009). A gene expression signature classifying telomerase and ALT immortalization reveals an hTERT regulatory network and suggests a mesenchymal stem cell origin for ALT. Oncogene *28*, 3765–3774.

Lin, M.T., and Beal, M.F. (2006). Mitochondrial dysfunction and oxidative stress in neurodegenerative diseases. Nature *443*, 787–795.

Lundblad, V., and Blackburn, E.H. (1993). An alternative pathway for yeast telomere maintenance rescues est1- senescence. Cell *73*, 347–360.

Maser, R.S., Choudhury, B., Campbell, P.J., Feng, B., Wong, K.K., Protopopov, A., O'Neil, J., Gutierrez, A., Ivanova, E., Perna, I., et al. (2007). Chromosomally unstable mouse tumours have genomic alterations similar to diverse human cancers. Nature *447*, 966–971.

Murphy, M.P. (2009). How mitochondria produce reactive oxygen species. Biochem. J. *417*, 1–13.

Nakamura, T.M., Morin, G.B., Chapman, K.B., Weinrich, S.L., Andrews, W.H., Lingner, J., Harley, C.B., and Cech, T.R. (1997). Telomerase catalytic subunit homologs from fission yeast and human. Science *277*, 955–959.

O'Hagan, R.C., Chang, S., Maser, R.S., Mohan, R., Artandi, S.E., Chin, L., and DePinho, R.A. (2002). Telomere dysfunction provokes regional amplification and deletion in cancer genomes. Cancer Cell *2*, 149–155.

Oexle, K., and Zwirner, A. (1997). Advanced telomere shortening in respiratory chain disorders. Hum. Mol. Genet. *6*, 905–908.

Potts, P.R., and Yu, H. (2007). The SMC5/6 complex maintains telomere length in ALT cancer cells through SUMOylation of telomere-binding proteins. Nat. Struct. Mol. Biol. *14*, 581–590.

Qi, L., Strong, M.A., Karim, B.O., Armanios, M., Huso, D.L., and Greider, C.W. (2003). Short telomeres and ataxia-telangiectasia mutated deficiency cooperatively increase telomere dysfunction and suppress tumorigenesis. Cancer Res. *63*, 8188–8196.

Retèl, J., Hoebee, B., Braun, J.E., Lutgerink, J.T., van den Akker, E., Wanamarta, A.H., Joenje, H., and Lafleur, M.V. (1993). Mutational specificity of oxidative DNA damage. Mutat. Res. *299*, 165–182.

Rudolph, K.L., Millard, M., Bosenberg, M.W., and DePinho, R.A. (2001). Telomere dysfunction and evolution of intestinal carcinoma in mice and humans. Nat. Genet. *28*, 155–159.

Saharia, A., and Stewart, S.A. (2009). FEN1 contributes to telomere stability in ALT-positive tumor cells. Oncogene *28*, 1162–1167.

Sahin, E., and DePinho, R.A. (2010). Linking functional decline of telomeres, mitochondria and stem cells during ageing. Nature *464*, 520–528.

Sahin, E., Colla, S., Liesa, M., Moslehi, J., Müller, F.L., Guo, M., Cooper, M., Kotton, D., Fabian, A.J., Walkey, C., et al. (2011). Telomere dysfunction induces metabolic and mitochondrial compromise. Nature *470*, 359–365.

Shay, J.W., and Wright, W.E. (2006). Telomerase therapeutics for cancer: challenges and new directions. Nat. Rev. Drug Discov. *5*, 577–584.

St-Pierre, J., Drori, S., Uldry, M., Silvaggi, J.M., Rhee, J., Jäger, S., Handschin, C., Zheng, K., Lin, J., Yang, W., et al. (2006). Suppression of reactive oxygen species and neurodegeneration by the PGC-1 transcriptional coactivators. Cell *127*, 397–408.

Takai, H., Smogorzewska, A., and de Lange, T. (2003). DNA damage foci at dysfunctional telomeres. Curr. Biol. *13*, 1549–1556.

van Steensel, B., Smogorzewska, A., and de Lange, T. (1998). TRF2 protects human telomeres from end-to-end fusions. Cell *92*, 401–413.

Vander Heiden, M.G., Cantley, L.C., and Thompson, C.B. (2009). Understanding the Warburg effect: the metabolic requirements of cell proliferation. Science *324*, 1029–1033.

Warburg, O. (1956). On the origin of cancer cells. Science *123*, 309–314.

Weinberg, F., Hamanaka, R., Wheaton, W.W., Weinberg, S., Joseph, J., Lopez, M., Kalyanaraman, B., Mutlu, G.M., Budinger, G.R., and Chandel, N.S. (2010). Mitochondrial metabolism and ROS generation are essential for Kras-mediated tumorigenicity. Proc. Natl. Acad. Sci. USA *107*, 8788–8793.

Wiedemeyer, W.R., Dunn, I.F., Quayle, S.N., Zhang, J., Chheda, M.G., Dunn, G.P., Zhuang, L., Rosenbluh, J., Chen, S., Xiao, Y., et al. (2010). Pattern of retinoblastoma pathway inactivation dictates response to CDK4/6 inhibition in GBM. Proc. Natl. Acad. Sci. USA *107*, 11501–11506.

Wise, D.R., DeBerardinis, R.J., Mancuso, A., Sayed, N., Zhang, X.Y., Pfeiffer, H.K., Nissim, I., Daikhin, E., Yudkoff, M., McMahon, S.B., and Thompson, C.B. (2008). Myc regulates a transcriptional program that stimulates mitochondrial glutaminolysis and leads to glutamine addiction. Proc. Natl. Acad. Sci. USA *105*, 18782–18787.

Wong, K.K., Maser, R.S., Bachoo, R.M., Menon, J., Carrasco, D.R., Gu, Y., Alt, F.W., and DePinho, R.A. (2003). Telomere dysfunction and Atm deficiency compromises organ homeostasis and accelerates ageing. Nature *421*, 643–648.

Xu, Y., Ashley, T., Brainerd, E.E., Bronson, R.T., Meyn, M.S., and Baltimore, D. (1996). Targeted disruption of ATM leads to growth retardation, chromosomal fragmentation during meiosis, immune defects, and thymic lymphoma. Genes Dev. *10*, 2411–2422.

Yuneva, M., Zamboni, N., Oefner, P., Sachidanandam, R., and Lazebnik, Y. (2007). Deficiency in glutamine but not glucose induces MYC-dependent apoptosis in human cells. J. Cell Biol. *178*, 93–105.

Zeng, S., Xiang, T., Pandita, T.K., Gonzalez-Suarez, I., Gonzalo, S., Harris, C.C., and Yang, Q. (2009). Telomere recombination requires the MUS81 endonuclease. Nat. Cell Biol. *11*, 616–623.

Zhong, Z.H., Jiang, W.Q., Cesare, A.J., Neumann, A.A., Wadhwa, R., and Reddel, R.R. (2007). Disruption of telomere maintenance by depletion of the MRE11/RAD50/NBS1 complex in cells that use alternative lengthening of telomeres. J. Biol. Chem. *282*, 29314–29322.

Cell

EXTENDED EXPERIMENTAL PROCEDURES

Mice

Atm, *Terc* and *TERT-ER* mice described previously (Jaskelioff et al., 2011; Maser et al., 2007; Wong et al., 2003) were interbred and backcrossed to high grade of C57BL/6 (over 95%). The mating strategy to obtain experimental cohorts G_0, G_1 and G_{3-4} is shown in Figure S1A. 4-OHT time release pellets (5 mg; Innovative Research of America) were inserted subcutaneously at age of 18 weeks to reach steady state blood levels of 1 ng ml^{-1} 4-OHT for 60 consecutive days. Mice were maintained in specific pathogen-free (SPF) conditions at Dana-Farber Cancer Institute followed for lymphoma development. All experiments were performed with IACUC approval.

Histology, Tumor Characterization, and Sample Preparation

Mice with sign of thymic lymphomas were dissected, and multiple tissues including thymic tumor, brain, liver, lung, kidney, spleen, intestine and bone marrow were fixed with 10% formalin for 24 hr followed by 70% ethanol. Tissues were embedded in paraffin (Brigham and Women's Hospital), and sections were used for hematoxylin and eosin staining, β-gal staining and chromogenic immunohistochemistry (IHC). Antibodies used for IHC include anti-Ki67 (Dako), anti-53BP1 (Bethyl Labs), anti-γH2AX (Bethyl Labs) and anti-Cleaved Caspase 3 (Cell Signaling). Tumors were partitioned for DNA, RNA and protein extraction, and for in vitro culture. For FACS analysis, cells were separated from the tumors, immunostained with CD4, CD8 and CD3 antibodies (eBioscience) and analyzed on a BD FACSCanto II (BD Biosciences).The primary tumor sizes were obtained from the average of measurements at three dimensions.

Cell Culture and Cytogenetic Analysis

Tumor cells were separated from primary tumors and cultured in RPMI with 50 μM β-mercaptoethanol, 10% Cosmic Calf serum (HyClone), 0.5 ng ml^{-1} IL-2 (Peprotech), and 4 ng ml^{-1} IL-7 (Peprotech). For metaphase preparation, metaphases were obtained from colcemid-treated cells incubated in 105 mM KCl hypotonic buffer for 15 min before fixation in 3:1 methanol–acetic acid. Spectral karyotyping (SKY) was done using the SkyPaint Kit and SkyView analytical software (Applied Spectral Imaging) according to manufacturer's protocols. Chromosome aberrations were defined in accordance with the Committee on Standard Genetic Nomenclature for Mice. For telomere-FISH (fluorescent in situ hybridization), metaphase spreads were made on positively charged slides, dehydrated in cold ethanol series and air-dried. Slides were then denatured in 4% formaldehyde at 37°C for 2 min, applied with telomere-specific T_2AG_3-FITC PNA (peptide nucleic acid) probes and centromere-specific Cent-Cy3 or Cent-pacific blue PNA probes, post-denatured at 80°C, and hybridized at 4°C for 4 hr. Slides were then washed and counter-stained with DAPI (for microscopy) or TOTO3 (for laser scanning). Laser scanning cytometry quantification was performed with an iCys Research Imaging Cytometer (Compucyte) as described earlier (Jaskelioff et al., 2011; Sahin et al., 2011).

Telomere Sister Chromatid Exchange Assay

Telomere Co-FISH staining was performed as previously described (Potts and Yu, 2007). Specifically, cells were treated with 10 mM bromodeoxyuridine (brdU) for 16 hr, and metaphase spreads were made as described in "cell culture and cytogenetic analysis" section, followed by 0.5 mg ml-1 RNase A treatment for 10 min. Slides were incubated in 2 X SSC containing 10 μg ml^{-1} Hoescht 33258 for 15 min, and then exposed to 365-nm UV light (Stratalinker 1800) for 30 min. Nicked DNAs were then degraded by incubation of slides in 1.6% (v/v) ExoIII (Promega) for 10 min. Telomere Co-FISH with TelC-FAM PNA probe followed by TelG-Cy3 PNA probe was then performed on these slides as described in "cell culture and cytogenetic analysis" section.

RT-qPCR, Mitochondria DNA Content Measurement, and Western Blotting

DNA-free total RNA extracted from primary tumors or tumor cells with the RNeasy kit (QIAGEN) was used to prepare oligo-dT complementary DNA with Superscript III (Invitrogen). RT-qPCR primers are described in Table S4. Total DNAs were prepared with the PureGene kit (Gentra Systems), and mitochondria DNA content was measured by the relative levels of CoxI versus beta globin by qPCR. CoxI and beta globin primers are described in Table S4. Antibodies used for Western blotting are anti-phospho p53 (ser15, Cell Signaling), anti-p21 (Santa Cruz Biotechnology), anti-Vinculin (Sigma) and anti-Mre11 (BD Biosciences).

shRNA Knockdown

Lentiviral based shRNA constructs targeting mouse PGC-1β and SOD2 were ordered from The Dana-Farber/Harvard Cancer Center DNA Resource Core. Verified shRNA sequences were cloned into inducible lentiviral constructs PLKO-TRC-901 (IPTG inducible; Broad Institute) and (Doxycycline inducible; Novartis). The hairpin sequences used in this study are: PGC-1β-1: CCGGCGAGCTTTCACTGCTACAGAACTCGAGTTCTGTAGCAGTGAAAGCTCGTTTTTG; PGC-1β-2: CCGGCGGGAACTAAAGAAGCGCTTTCTCGAGAAAGCGCTTCTTTAGTTCCCGTTTTTG; SOD2-1: CCGGGAGGCTATCAAGCGTGACTTTCTCGAGAAAGTCACGCTTGATAGCCTCTTTTTG; SOD2-2: CCGGGCCACACATTAACGCGCAGATCTCGAGATCTGCGCGTTAATGTGTGGCTTTTTG.

Array-CGH Profiling and Analyses

For Array-CGH, genomic DNA processing, labeling and hybridization to Agilent CGH 60-mer oligo arrays were performed as per the manufacturer's protocol (http://www.agilent.com). Labeled DNAs were hybridized onto 244K and 415K microarrays, against matched tail DNA. Fluorescence ratios of scanned images were normalized and averaged from two pairs (dye swap), and copy number profile was generated by Circular Binary Segmentation, which determines significance of change points in raw data through permutation (Olshen et al., 2004).

SGOL scores were calculated for genes using the SGOL function of the cghMCR package of the Bioconductor project (Wiedemeyer et al., 2010). The algorithm applies the GISTIC (Beroukhim et al., 2007) approach of summarizing copy number alterations across multiple samples to segmented data to speed up the computation for high density arrays and facilitate integration of data from different platforms (e.g., 244K and 415K custom arrays in this case; Agilent). We took the gene-centric approach by assigning the segment value to genes within the segment for all of the segments identified for each sample and then summarize the derived values per gene across all of the samples using thresholds of 0.4 and −0.4 for gains and losses, respectively, to generate the SGOL scores. High absolute SGOL scores indicate high frequency and/or magnitude of alterations across samples.

Homolog mapping: genes within mouse T cell lymphomas identified with SGOL algorithm were used to obtain their human homolog on the basis of the NCBI homologene website (http://www.ncbi.nlm.nih.gov.ezp-prod1.hul.harvard.edu/entrez/query.fcgi?db = homologene).

Permutation testing: permutation testing was conducted for statistical significance of cross-species overlap by randomly generating a simulated mouse genome containing the same number in the corresponding chromosomes as the actual mouse genome; a similar set was created for human T-ALL data set (Maser et al., 2007). The number of overlapping genes between mouse and each human genome was calculated and stored, and repeated 10,000 times independently for amplifications and deletions. The *P* value for significance of overlap for each was calculated by dividing the frequency of randomly achieved overlap by 10,000.

Pathway Analysis

891 upregulated and 1345 downregulated genes with 1.5 fold change and $p < 0.01$ in ALT+ tumors relative to telomerase+ tumors were applied with Knowledge-based Pathway (IPA) analysis. The significantly represented pathways were compared with the pathways obtained from the similar analysis on 10 ALT+ and 8 telomerase+ osteosarcomas (Lafferty-Whyte et al., 2009). Overlapped pathways are listed.

Mitochondrial Oxygen Consumption Measurements in Live Cells

Cells were grown in seahorse medium with 5.5 mM Glucose and 0.1 mM Pyruvate (pH 7.4, no HEPES) for overnight in 37°C incubator without CO_2. Seahorse plate were coated with 30 ml sterile 50 μg ml^{-1} poly-D lysine per well for 1 hr, wash it with 300 ml H2O, and then let it dry inside the hood for 1 hr. Two million cells per well were seeded in 700 μl seahorse medium one hour before the experiment. The plate was centrifuged at 450 rpm for 5 min and with gradual stop (no brakes used to stop the rotor), and then the plate was re-oriented at opposite direction and re-centrifuged at 650 rpm for 5 min. The plate was placed in a 37°C incubator without CO_2 for 50 min after centrifugation. Oxygen consumption rates (OCRs) were measured using the Seahorse XF24 instrument (Seahorse Biosciences). Basal mitochondrial respiration were measured at four time points, and respiration non-linked to mitochondrial ATP synthesis were measured at four time points after adding 1 μM oligomycin. Non-mitochondrial OCRs were obtained by adding 5 μM antimycin A, and uncoupled respiration was obtained by adding 1 μM FCCP.

ROS Measurement

For determination of ROS levels, tumor cells were stained with 5 μM CM-H_2DFCDA (Invitrogen) at 37°C for 30 min, followed by FACS analysis on a BD FACSCanto II (BD Biosciences). FACS profiles were edited on FlowJo software, and means of the curves were obtained.

COX Model Test

Effects of shPGC-1β knockdown on Tel+ and ALT+ cells were tested by Cox analysis. R function Coxph() proportional hazards model was applied: Y = b1X1 + b2X2 + b3X1*X2, where Y is generated by R function Surv() using the survival data; X1 is the status variable of whether the cell line is ALT; X2 is the status variable of the PGC1β knockdown. The null hypothesis is that there is no combined effect of ALT and PGC-1β knockdown on the survival rate. We obtained a p-value of 0.0065 that suggests whether the cell line is ALT has a significant effect on the survival rate under PGC-1β knockdown.

SUPPLEMENTAL REFERENCES

Beroukhim, R., Getz, G., Nghiemphu, L., Barretina, J., Hsueh, T., Linhart, D., Vivanco, I., Lee, J.C., Huang, J.H., Alexander, S., et al. (2007). Assessing the significance of chromosomal aberrations in cancer: methodology and application to glioma. Proc. Natl. Acad. Sci. USA *104*, 20007–20012.

Jaskelioff, M., Muller, F.L., Paik, J.H., Thomas, E., Jiang, S., Adams, A.C., Sahin, E., Kost-Alimova, M., Protopopov, A., Cadinanos, J., et al. (2011). Telomerase reactivation reverses tissue degeneration in aged telomerase-deficient mice. Nature *469*, 102–106.

Lafferty-Whyte, K., Cairney, C.J., Will, M.B., Serakinci, N., Daidone, M.G., Zaffaroni, N., Bilsland, A., and Keith, W.N. (2009). A gene expression signature classifying telomerase and ALT immortalization reveals an hTERT regulatory network and suggests a mesenchymal stem cell origin for ALT. Oncogene *28*, 3765–3774.

Maser, R.S., Choudhury, B., Campbell, P.J., Feng, B., Wong, K.K., Protopopov, A., O'Neil, J., Gutierrez, A., Ivanova, E., Perna, I., et al. (2007). Chromosomally unstable mouse tumours have genomic alterations similar to diverse human cancers. Nature *447*, 966–971.

Olshen, A.B., Venkatraman, E.S., Lucito, R., and Wigler, M. (2004). Circular binary segmentation for the analysis of array-based DNA copy number data. Biostatistics *5*, 557–572.

Potts, P.R., and Yu, H. (2007). The SMC5/6 complex maintains telomere length in ALT cancer cells through SUMOylation of telomere-binding proteins. Nat. Struct. Mol. Biol. *14*, 581–590.

Sahin, E., Colla, S., Liesa, M., Moslehi, J., Muller, F.L., Guo, M., Cooper, M., Kotton, D., Fabian, A.J., Walkey, C., et al. (2011). Telomere dysfunction induces metabolic and mitochondrial compromise. Nature *470*, 359–365.

Wiedemeyer, W.R., Dunn, I.F., Quayle, S.N., Zhang, J., Chheda, M.G., Dunn, G.P., Zhuang, L., Rosenbluh, J., Chen, S., Xiao, Y., et al. (2010). Pattern of retinoblastoma pathway inactivation dictates response to CDK4/6 inhibition in GBM. Proc. Natl. Acad. Sci. USA *107*, 11501–11506.

Wong, K.K., Maser, R.S., Bachoo, R.M., Menon, J., Carrasco, D.R., Gu, Y., Alt, F.W., and DePinho, R.A. (2003). Telomere dysfunction and Atm deficiency compromises organ homeostasis and accelerates ageing. Nature *421*, 643–648.

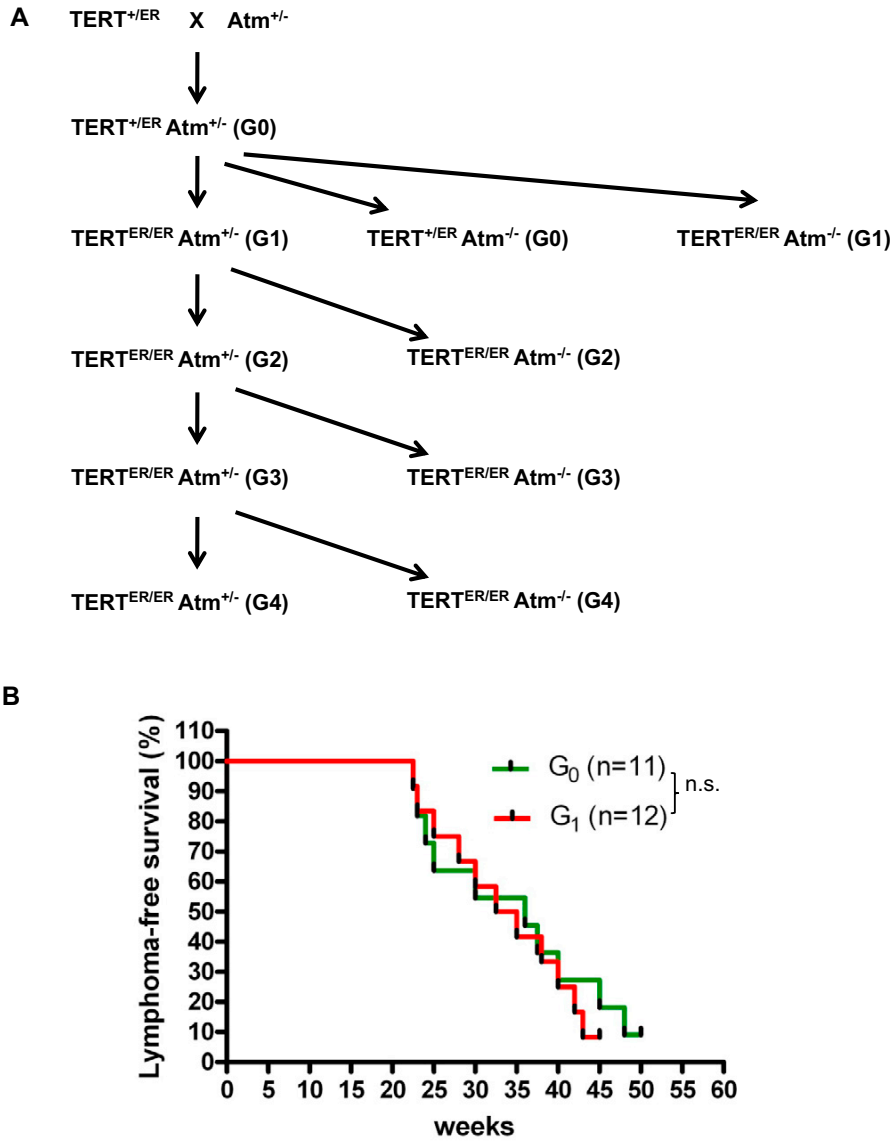

Figure S1. Mating Strategy, Related to Figure 1

(A) Mating strategy to get experimental cohorts G_0 *Atm*$^{-/-}$ *TERT*$^{+/+ \text{ or } +/ER}$, G_1 *Atm*$^{-/-}$ *TERT*$^{ER/ER}$, $G_{3\text{-}4}$ *Atm*$^{-/-}$*TERT*$^{ER/ER}$ mice.

(B) The G_0 and G_1 mice developed T cell lymphomas at similar latencies and penetrance.

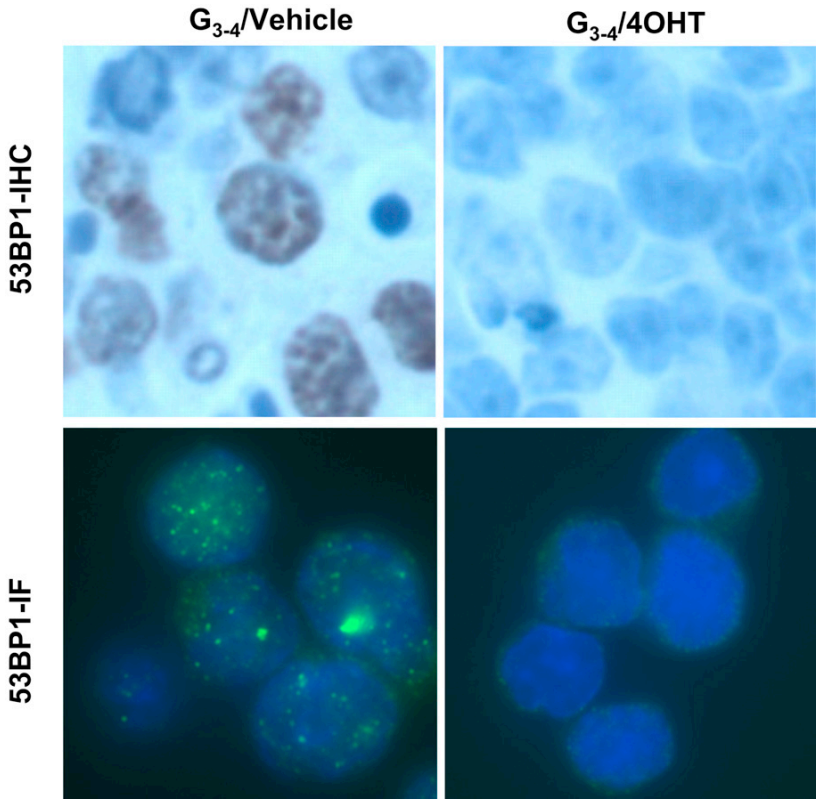

Figure S2. IHC and IF Staining of 53BP1 in G_{3-4} Tumors with 4-OHT and Vehicle Treatment, Related to Figure 2

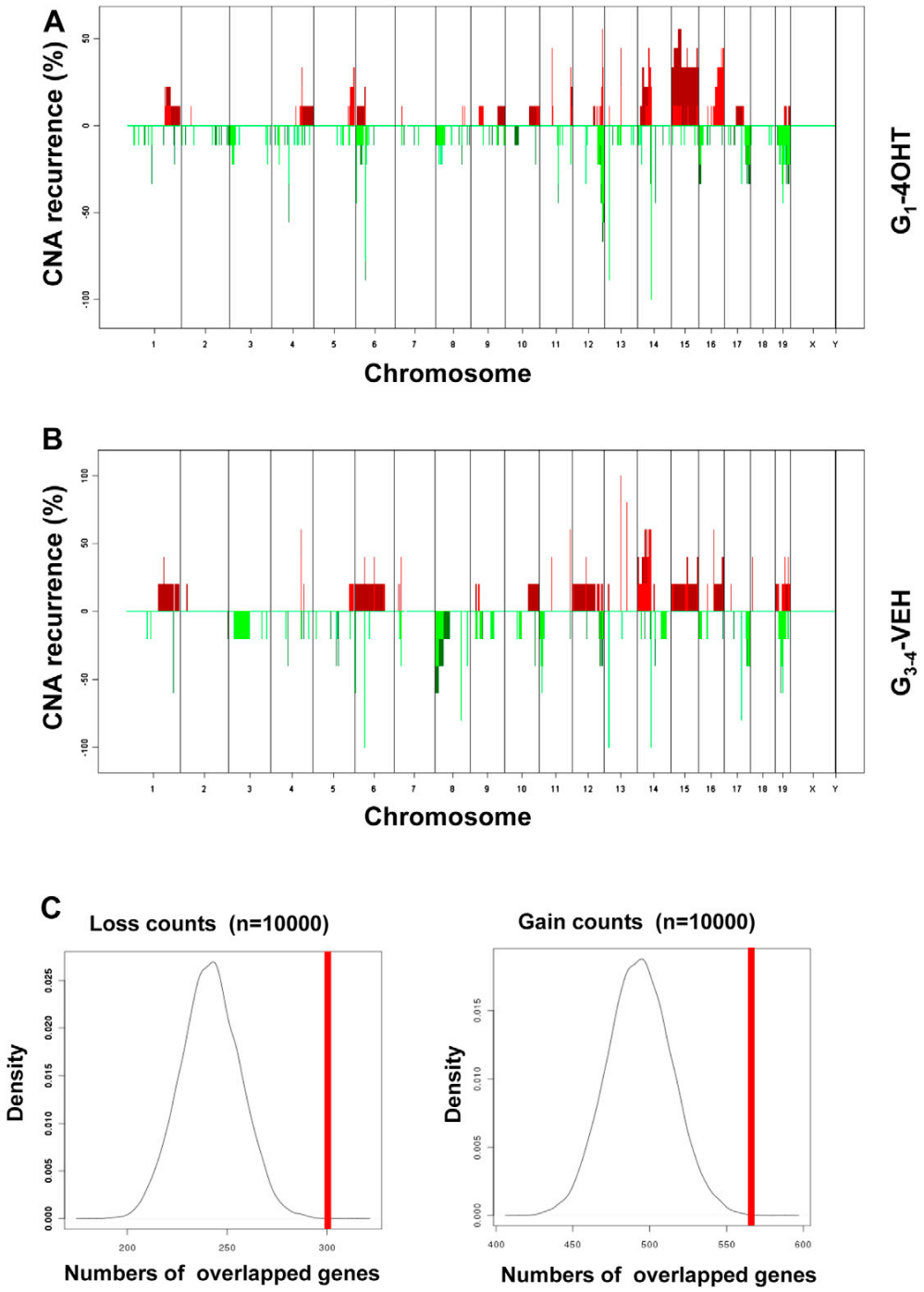

Figure S3. Telomerase Reactivation Promotes Invasiveness of Late-Generation *TERT*$^{ER/ER}$ *Atm*$^{-/-}$ Lymphomas, Related to Figure 3

(A) Recurrence plot of CNAs defined by array-CGH for 10 G_1-4-OHT lymphomas.

(B) Recurrence plot of CNAs defined by array-CGH for 5 G_{3-4}-VEH lymphomas

(C) Genes in CNAs of G_{3-4}-4-OHT tumors (4928 for gain and 2297 for loss) and human T-ALL (4470 for gain and 3885 for loss) identified with SGOL algorithm were compared. Red lines indicate the numbers of overlapping (565 for gain and 300 for loss). Same numbers of randomly picked genes from mouse and human tumors were compared 10,000 times and the numbers of overlapped genes were plotted.

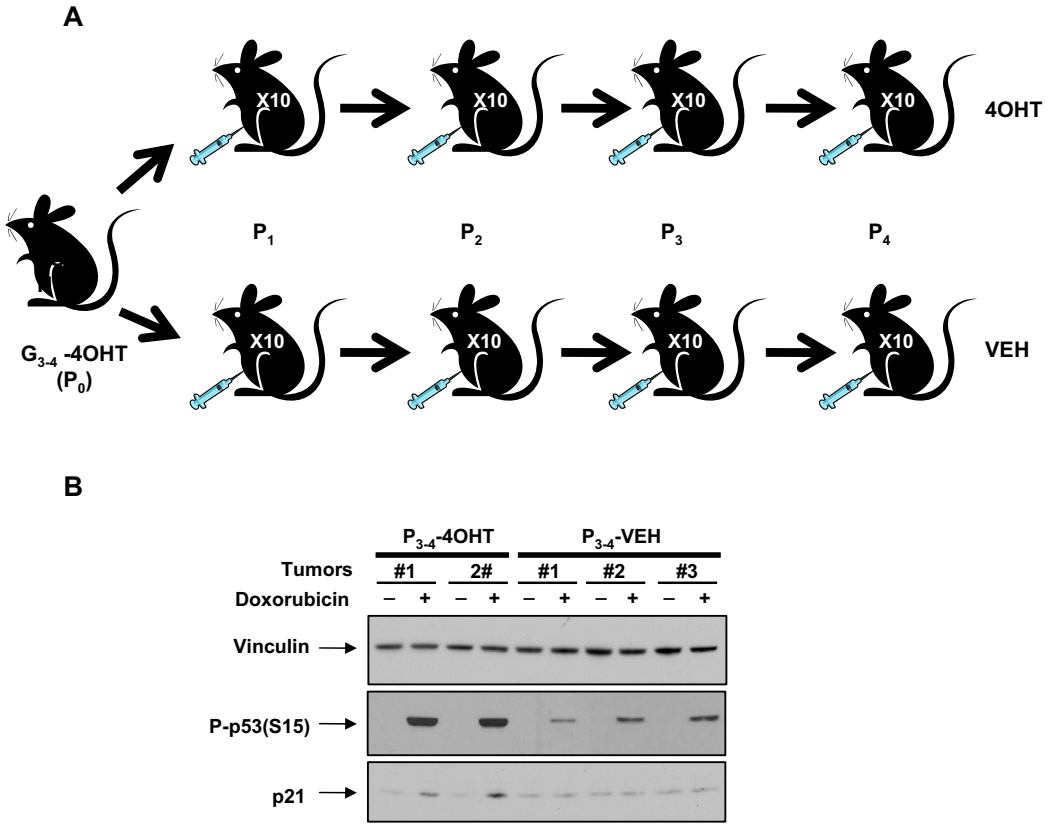

Figure S4. Telomerase Depletion in Late-Generation 4-OHT-*TERT*$^{ER/ER}$ *Atm*$^{-/-}$ Lymphomas Leads to Cell Death and Resistance, Related to Figure 4

(A) Strategy to assess telomerase extinction in $G_{3\text{-}4}$ tumors. Freshly harvested tumor cells from 4-OHT-treated $G_{3\text{-}4}$ mice were passaged directly through SCID mice that were pre-implanted with vehicle or 4-OHT tablets (10 mice per each passage of treatment; 10^7 cells per intraperitoneal injection).

(B) Immunoblotting of phosphorylated p53 (S15) and p21 in $G_{3\text{-}4}$-4-OHT lymphomas and $G_{3\text{-}4}$-VEH resistant tumors.

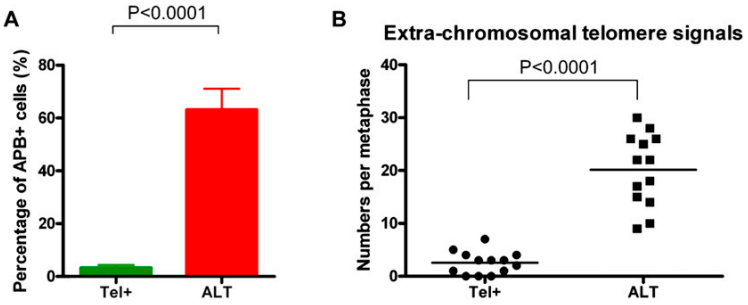

Figure S5. ALT Features in Two Tumors with Early ALT Acquisition, Related to Figure 5

(A) Quantification of ALT-associated PML Body (APB) numbers in two tumors with early ALT acquisition (n = 2 for ALT+ and n = 3 for telomerase+).
(B) Quantification of extra-chromosomal telomere fragments in two tumors with early ALT acquisition (n = 2 for ALT+ and n = 3 for telomerase+).
t test was used to calculate the statistical significance, and error bars indicate s.d.

A

Up in ALT		Down in ALT	
Canonical pathway	Tox list	Canonical pathway	Tox list
SAPK/JNK Signaling	Increases Transmembrane Potential of Mitochondria and Mitochondrial Membrane	Regulation of eIF4 and p70S6K Signaling	p53 Signaling
Huntington's Disease Signaling	PPARα/RXRα Activation	EIF2 Signaling	Cell Cycle: G1/S Checkpoint Regulation
B Cell Receptor Signaling	RAR Activation	Molecular Mechanisms of Cancer	Cardiac Necrosis/Cell Death
LPS-stimulated MAPK Signaling	Cardiac Fibrosis	Myc Mediated Apoptosis Signaling	Pro-Apoptosis
TWEAK Signaling	Liver Necrosis/Cell Death	mTOR Signaling	
TNFR1 Signaling	Oxidative Stress	Cell Cycle: G1/S Checkpoint Regulation	
PTEN Signaling	Hepatic Stellate Cell Activation	Non-Small Cell Lung Cancer Signaling	
HER-2 Signaling in Breast Cancer		p53 Signaling	
PPARα/RXRα Activation		Chronic Myeloid Leukemia Signaling	
Glucocorticoid Receptor Signaling		Glioma Invasiveness Signaling	

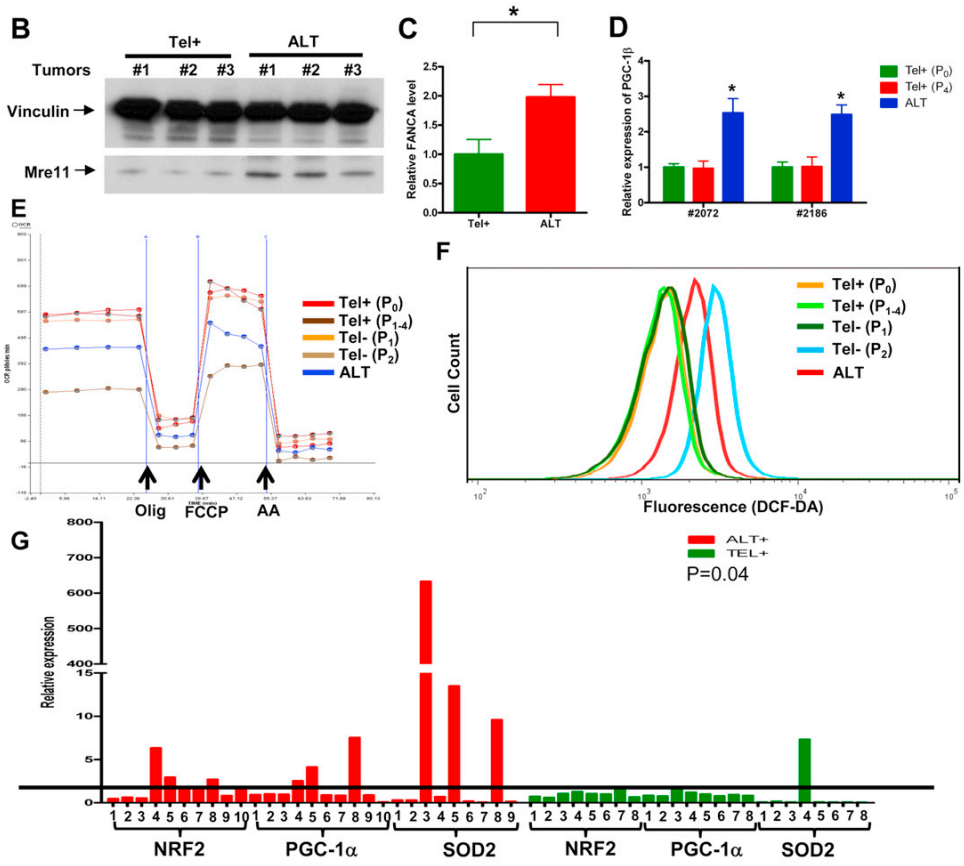

Figure S6. Pathways and Genes Changed in ALT+ Tumors Relative and Telomerase+ Tumors, Related to Figure 6

(A) Pathways that are significantly represented in both G_{3-4} ALT+ tumors and human ALT+ osteosarcomas (Lafferty-Whyte et al., 2009).

(B) Immunoblotting of Mre11 protein in G_{3-4} telomerase+ and ALT+ tumors.

(C) Measurement of FANCA expression levels in G_{3-4} telomerase+ and ALT+ tumors with RT-qPCR.

(D) Measurement of PGC-1β expression levels in two other independent telomerase+ and ALT+ tumors with RT-qPCR.

(E) Representative Oxygen Consumption Rates (OCRs) curves measured in serially transplanted lymphomas and ALT+ lymphomas.

(F) Representative profiles of ROS levels in serially transplanted lymphomas and ALT+ lymphomas measured by DCFDA staining followed by FACS analysis.

(G) Relative levels of PGC-1α, NRF2 and SOD2 in 10 human ALT+ and 8 telomerase+ osteosarcomas were normalized for the average levels of telomerase+ osteosarcomas. Raw data were obtained from the transcriptomic profiles (Lafferty-Whyte et al., 2009).

t test was used to calculate the statistical significance of (C), (D) and (G), and error bars indicate s.d. (*p < 0.0001).

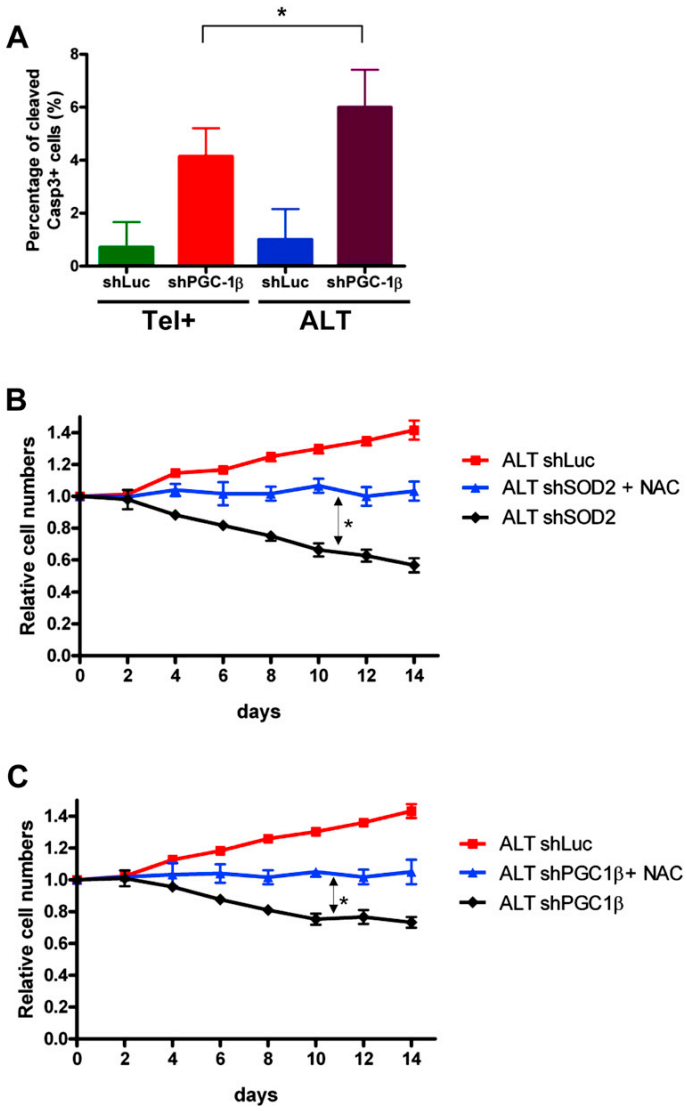

Figure S7. Inhibition of PGC-1β or SOD2 Differentially Kills ALT+ Tumors over Telomerase+ Tumors, Related to Figure 7

(A) Percentage of cleaved Caspase 3 positive cells in Telomerase+ and ALT+ tumors with PGC-1β or control knockdown. t test was used to calculate the statistical significance, and error bars indicate s.d. (*p = 0.01).

(B) Relative cells numbers of ALT+ tumor cells with SOD2 shRNAs or/and NAC treatment (n = 3). Two way ANOVA was used to calculate the statistical significance (*p < 0.0001).

(C) Relative cells numbers of ALT+ tumor cells with PGC-1β shRNAs or/NAC treatment (n=3). Two way ANOVA was used to calculate the statistical significance (p< 0.001).